10-3-2009

Cryo-Electron Tomography Elucidates the Molecular Architecture of Treponema pallidum, the Syphilis Spirochete

Jacques Izard

Christian Renken

Chyong-Ere Hsieh

Daniel C. Desrosiers

Star Dunham-Ems

See next page for additional authors

Authors

Jacques Izard, Christian Renken, Chyong-Ere Hsieh, Daniel C. Desrosiers, Star Dunham-Ems, Carson La Vake, Linda L. Gebhardt, Ronald J. Limberger, David L. Cox, Michael Marko, and Justin D. Radolf

JOURNAL OF BACTERIOLOGY, Dec. 2009, p. 7566–7580 Vol. 191, No. 24
0021-9193/09/$12.00 doi:10.1128/JB.01031-09

Cryo-Electron Tomography Elucidates the Molecular Architecture of *Treponema pallidum*, the Syphilis Spirochete▽†

Jacques Izard,[1,2]¶ Christian Renken,[3]¶‡ Chyong-Ere Hsieh,[3]¶ Daniel C. Desrosiers,[4] Star Dunham-Ems,[4] Carson La Vake,[4] Linda L. Gebhardt,[3] Ronald J. Limberger,[3] David L. Cox,[6] Michael Marko,[3] and Justin D. Radolf[4,5]*

Department of Molecular Genetics, The Forsyth Institute, Boston, Massachusetts 02135[1]; Harvard School of Dental Medicine, Boston, Massachusetts 02115[2]; Wadsworth Center, New York State Department of Health, Albany, New York 12201[3]; Departments of Medicine[4] and Genetics and Developmental Biology,[5] University of Connecticut Health Center, Farmington, Connecticut 06030; and Division of STD Prevention, Laboratory Reference and Research Branch, Centers for Disease Control and Prevention, Atlanta, Georgia 30333[6]

Received 4 August 2009/Accepted 3 October 2009

Cryo-electron tomography (CET) was used to examine the native cellular organization of *Treponema pallidum*, the syphilis spirochete. *T. pallidum* cells appeared to form flat waves, did not contain an outer coat and, except for bulges over the basal bodies and widening in the vicinity of flagellar filaments, displayed a uniform periplasmic space. Although the outer membrane (OM) generally was smooth in contour, OM extrusions and blebs frequently were observed, highlighting the structure's fluidity and lack of attachment to underlying periplasmic constituents. Cytoplasmic filaments converged from their attachment points opposite the basal bodies to form arrays that ran roughly parallel to the flagellar filaments along the inner surface of the cytoplasmic membrane (CM). Motile treponemes stably attached to rabbit epithelial cells predominantly via their tips. CET revealed that *T. pallidum* cell ends have a complex morphology and assume at least four distinct morphotypes. Images of dividing treponemes and organisms shedding cell envelope-derived blebs provided evidence for the spirochete's complex membrane biology. In the regions without flagellar filaments, peptidoglycan (PG) was visualized as a thin layer that divided the periplasmic space into zones of higher and lower electron densities adjacent to the CM and OM, respectively. Flagellar filaments were observed overlying the PG layer, while image modeling placed the PG-basal body contact site in the vicinity of the stator–P-collar junction. Bioinformatics and homology modeling indicated that the MotB proteins of *T. pallidum*, *Treponema denticola*, and *Borrelia burgdorferi* have membrane topologies and PG binding sites highly similar to those of their well-characterized *Escherichia coli* and *Helicobacter pylori* orthologs. Collectively, our results help to clarify fundamental differences in cell envelope ultrastructure between spirochetes and gram-negative bacteria. They also confirm that PG stabilizes the flagellar motor and enable us to propose that in most spirochetes motility results from rotation of the flagellar filaments against the PG.

Spirochetes are an ancient and extremely successful eubacterial phylum characterized by distinctive helical or planar wave-form morphology and flagellar filaments confined to the periplasmic space (55, 87). Spirochetes from the genera *Leptospira*, *Treponema*, and *Borrelia* are highly invasive pathogens that pose public health problems of global dimensions (1, 6, 57, 109). *Treponema denticola* and numerous other treponemal species, most of which remain uncultivated, are major components of the polymicrobial biofilms that cause periodontal disease (34, 56) and also have been implicated as risk factors for atherosclerosis (4, 125). The treponemal symbionts that dwell in the hindguts of termites, where they provide their insect host with essential nutrients (10), are one of the most striking examples of the extraordinary biodiversity achieved by spirochetes. It is readily apparent, therefore, that in the course of their complex evolution, spirochetes have exploited a basic ultrastructural plan to accommodate an immense spectrum of metabolic activities and lifestyles, both commensal and pathogenic.

Venereal syphilis is a multistage, sexually transmitted disease caused by the noncultivatable spirochete *Treponema pallidum*. Following inoculation, usually in the genital region, *T. pallidum* disseminates via lymphatics and blood to diverse organs, where it can establish persistent, even life-long, infection (68, 97). Over the years there has been great interest in defining ultrastructural features of the syphilis spirochete that might contribute to syphilis pathogenesis (58, 64, 84, 120, 121). Classic electron microscopy studies established that *T. pallidum* possesses a characteristic spirochete ultrastructure consisting of outer and cytoplasmic membranes and periplasmic flagellar filaments originating from cytoplasmic membrane-associated, subterminal basal bodies (55, 58). Hovind-Hougen (58) identified a putative peptidoglycan (PG) layer surrounding the cytoplasmic membrane (CM), and she noted that the end of the bacterium contains a distinct structural entity which she

* Corresponding author. Mailing address: The University of Connecticut Health Center, 263 Farmington Avenue, Farmington, CT 06030-3715. Phone: (860) 679-8480. Fax: (860) 679-1358. E-mail: JRadolf@up.uchc.edu.

† Supplemental material for this article may be found at http://jb.asm.org/.

¶ J.I., C.R., and C.-E.H. contributed equally to this work.

‡ Present address: Applied Biophysics, Inc., Troy, NY 12180.

▽ Published ahead of print on 9 October 2009.

speculated mediates polar attachment to mammalian cells and extracellular matrix components. Freeze-fracture analysis has shown that the *T. pallidum* outer membrane (OM) contains a lower density of membrane-spanning proteins than its counterparts in either gram-negative bacteria or cultivatable spirochetes (99, 118), and it is thought that the paucity of surface-exposed antigenic targets resulting from this unusual OM ultrastructure is an important element of the spirochete's strategy for immune evasion (14, 93, 97).

In the more than 10 years since the publication of the *T. pallidum* genomic sequence made available a much-needed parts list for the bacterium (44), we have learned comparatively little about how these components are organized to create this extremely virulent and immunoevasive pathogen. Cryo-electron tomography (CET) has emerged as a powerful methodology for bridging the gap between protein-protein interactions and cellular architecture (70, 71). With this technique, thin films of cells are vitreously frozen to preserve cell structure in a close-to-native state, thereby avoiding chemical fixation, dehydration, and staining artifacts typically associated with conventional electron microscopy (EM). A series of images acquired as the sample is progressively tilted in an electron microscope are used to generate a three-dimensional (3D) reconstruction of the intact cell. In recent years, investigators have used CET to examine a variety of eukaryotic and prokaryotic cell types (70, 73, 77). With respect to spirochetes, CET has been used to visualize the intact flagellar motors of *Treponema primitia* (79) and *Borrelia burgdorferi* (67, 72); novel internal and external structural features of *T. denticola* (60); *Treponema primitia* (80), *B. burgdorferi* (66), and *Leptospira interrogans* (74); the flat ribbon configuration of *B. burgdorferi* periplasmic flagella (18); and the defects created in *B. burgdorferi* OMs when organisms are incubated with a borreliacidal monoclonal antibody (69). In the present study, we used CET to examine the native cellular organization of *T. pallidum*. These analyses demonstrated, not surprisingly, that *T. pallidum* shares many structural features with *T. denticola* while, at the same time, calling attention to the fluidity and dynamism of the syphilis spirochete's cell envelope. Our study also revealed that *T. pallidum* cell ends possess an unexpected degree of structural complexity and diversity compared to those of other spirochetes examined to date by CET. Lastly, our work has clarified the location of the PG layer within the periplasmic space and its spatial relationship to the motility apparatus, which are prerequisites for understanding spirochete movement and, by extension, invasiveness. As a whole, the information obtained underscores and clarifies fundamental differences in cell envelope composition and organization between *T. pallidum*, as well as other pathogenic spirochetes, and the model gram-negative bacterium, *Escherichia coli*.

MATERIALS AND METHODS

Bacterial strains. Male New Zealand White rabbits (approximately 3.5 kg) maintained on antibiotic-free food and water and housed at 16°C were inoculated by injection of each testis with 1×10^8 *T. pallidum*. Ten days later, the animals were euthanized and the testes were aseptically removed. Several lengthwise cuts were made in each testis, following which the treponemes were extracted on a rotary shaker in CMRL 1066 (Invitrogen, Carlsbad, CA) for cryo-electron microscopy or *T. pallidum* cultivation medium (23) for attachment experiments (see below). Gross testicular contaminants were removed from the extract by centrifugation at $400 \times g$ for 15 min. The animal protocols for this work were approved by the University of Connecticut Health Center Animal Care Committee and the Animal Care Committee of the Centers for Disease Control and Prevention under the auspices of Animal Welfare Assurance numbers A3471-01 and A4365-01, respectively. Virulent *B. burgdorferi* strain 297 (110) was propagated in BSK-II medium (3) supplemented with 6% normal rabbit serum (Pel-Freeze Biologicals, Rogers, AK) and temperature shifted as described previously (13).

Determination of *T. pallidum* shape. Freshly harvested treponemes were diluted in CMRL medium (GIBCO Invitrogen, Carlsbad, CA) containing 50 μg/ml protease inhibitor complex (Sigma Chemicals, St. Louis, MO) to a final concentration of 5×10^6 organisms/ml. Ten microliters of the suspension containing 5×10^6 organisms/ml was transferred to a clean microscope slide, and the live organisms were imaged at 100× magnification (1.4 numerical aperture) using dark-field microscopy on an Olympus BX41 microscope equipped with a Retiga Exi charge-coupled-device camera (Q Imaging, Tucson, AZ). Treponemes also were labeled with FM4-64 (Invitrogen) by incubating the organisms in CMRL medium containing 500 ng/ml FM4-64 for 5 minutes (123); labeled organisms were imaged by epifluorescence microscopy at 100× magnification (1.4 numerical aperture) using a rhodamine filter set. *B. burgdorferi* cells grown to stationary phase following temperature shift were imaged using dark-field microscopy. Image analyses were performed using ImageJ (version 1.42; NIH) and Adobe Photoshop (version 7.0; Adobe Photosystems, Mountain View, CA).

Sample preparation for electron microscopy. (i) Cryo-electron tomography. EM specimen grids (R2/1 or R3.5/1; Quantifoil Microtools, Jena, Germany) were pretreated with a 10-nm colloidal gold solution to provide fiducial markers for alignment of the tomographic tilt series (88). *T. pallidum* suspensions were processed for CET within 4 h of extraction; at the time of sample preparation, spirochetes were confirmed to be highly motile and well dispersed by dark-field microscopy. Thin films of treponemal suspensions were applied to grids, blotted, and immediately plunge-frozen into liquid ethane at liquid nitrogen temperature (36). Grids were stored under liquid nitrogen.

(ii) Negative staining. One milliliter of freshly harvested *T. pallidum* suspension was centrifuged at $12{,}000 \times g$ at 4°C for 20 min, after which the pellet was resuspended in 1 ml of CMRL. The high-speed centrifugation and resuspension step was performed to increase the number of organisms with disrupted OMs (26). Sample droplets were placed on 200-mesh, butvar carbon-coated Cu/Rd grids, allowed to adsorb for 1 to 2 min, and negatively stained with 1% uranyl acetate for 1 to 2 min. Samples were observed using a JEOL JEM-100CX transmission electron microscope operated at an accelerating voltage of 60 kV.

Electron microscopy and tomographic reconstruction. Images were recorded at −178°C, using a JEOL JEM-4000FX microscope equipped with a Gatan GIF2002 energy filter. The microscope was operated at 400 kV acceleration voltage, in zero-loss energy-filtered mode. Single-axis tilt series were collected with a 1° increment and 120° angular range. The total electron dose for a tilt series was about 120 electrons/Å^2. The calculated resolution (28) in the *x-y* plane (parallel to the grid) was 6 to 10 nm, with the better resolution corresponding to thinner specimens. The calculated *z* (depth) resolution was 1.6 times the *x-y* resolution due to the limited tilt range in these single-tilt axis reconstructions (92). The underfocus value, 15 μm, was chosen to maximize the transfer of information in images at the expected resolution limit (76). All image processing was done using SPIDER (42), and the reconstructions were computed by weighted back-projection (91). A total of 176 cells were examined in this study. Eight treponemes were used for independent tomographic reconstructions, while the remainder of the cells were from high-dose single cryo-EM images.

Measurements and visualization. Measurements were limited to tomographic reconstructions. The reconstructed 3D volumes were viewed slice by slice in ImageJ (http://rsb.info.nih.gov/ij/). The ImageJ line tool was used to measure the distance between two points or the width of a feature. The original pixel size of the tilt series images, as well as the voxel size of the reconstructions, was 1.8 nm. All measurements were made on *x-y* plane slices, to avoid effects of elongation due to limited tilt range. Averages were determined by measuring features in 10 separate planes at five to eight regions for each of the tomograms and calculated using 0.1-nm precision and rounded to the nearest integer. Values are based on nominal instrument magnification with an expected accuracy of ±5%. Diameters of cells and cytoplasmic cylinders were measured in the mid-section of each cell in the horizontal plane, avoiding lateral regions containing flagellar filaments. The diameter of each flagellar filament was taken using the greatest width within a single slice, avoiding the effects of curvature; measurements were taken through the flagellar bundles of five of the tomograms and were repeated in slices above and below. Distances between the CM and OM were measured from the midpoints of each membrane. Likewise, CM-to-PG measurements were made from the midpoint of the CM to the midpoint of the PG density. Surface-rendered models and animations were created using segmentation routines in

amira (Visage Imaging, San Diego, CA). Basal body models were created by aligning three basal bodies using affine registration followed by averaging in amira (Visage Imaging, San Diego, CA). A cylindrical average was made in SPIDER using 5° rotations. The final cylindrical average was aligned to basal bodies in tomograms by the affine registration method in amira. To visualize the fit of the cylindrical average with multiple basal bodies within a single tomographic slice (as in Fig. 7h, below), composite slices needed to be made. For these images, boxes delineate areas of contribution from separate slices.

Attachment experiments. Freshly harvested spirochetes were enumerated by dark-field microscopy using a Hawksley (United Kingdom) counting chamber. In three independent experiments, four parallel cultures of Sf1Ep cells (23) were established in T-25 tissue culture flasks for enumeration of attached organisms by PCR and in six-well (10-cm^2) microtiter plates containing sterilized coverslips for evaluation of the mode of attachment of individual spirochetes by dark-field microscopy. T-25 flasks were seeded with 1×10^7 cells to achieve 50% confluence followed by incubation for 48 h at 37°C in Eagle's minimal essential medium containing 10% fetal calf serum. To establish time zero for the attachment experiments, the monolayers were washed and then overlaid with 1×10^6 *T. pallidum* organisms in *T. pallidum* cultivation medium to achieve a spirochete-to-cell ratio of 10:1. The number of organisms in each inoculum was determined initially by dark-field enumeration and subsequently confirmed by quantitative real-time PCR (see below). Cultures were equilibrated with 92% N_2, 5% CO_2, and 3% O_2, placed in a chamber containing the same gas mixture, and incubated at 34°C for 3 h. This time period was selected based on prior results in an in vitro attachment/invasion model (114) and because it was considered to be reflective of the interval required for the establishment of infection following the venereal transmission of treponemes (97). At the end of the incubation, the infected monolayers were washed three times with sterile phosphate-buffered saline (PBS) to remove any organisms that were not tightly bound. The culture medium and the three washings containing unattached organisms were pooled and saved for quantitative PCR analysis. The monolayers were removed from the bottom of the vessels using a sterile cell scraper and suspended in 1 ml of PBS. The wells were rinsed twice with 1 ml of PBS, and the collected rinses were pooled with the original sample. The cells containing attached treponemes as well as treponemes in the tissue culture medium and washings were each collected by centrifugation at $12{,}000 \times g$ for 20 min. DNA was extracted from each cell pellet using an EpiCentre kit (Epicentre Biotechnologies, Madison, WI). The Master Mix reagent kit for the real-time PCR assays was manufactured by Qiagen, and the assays were performed using a Stratagene (La Jolla, CA) Mx3000p instrument. Standard curves were established using a TaqMan assay for the *flaA* gene using a previously described primer pair and probe (33). Threshold cycle values obtained for the cell-associated and unattached treponemes were used to calculate the percentages of attached organisms.

For microscopic analysis, wells containing 5×10^5 of Sf1Ep cells were inoculated with 5×10^6 treponemes. After a 3-h incubation period, the monolayers were washed three times with PBS. The coverslips with attached monolayers were removed from the wells with sterile forceps, inverted onto a glass slide, and observed by dark-field microscopy. In each experiment at least 100 organisms from two different wells were observed and scored for their mode of attachment. Organisms were evaluated as to whether they were attached by a single tip, both tips, or horizontally attached. Digital images of treponemes attached to cells on glass coverslips were captured using a SPOT Insight 12 camera (Diagnostic Instruments, Inc., Sterling Heights, MI) mounted to a Nikon Eclipse E400 microscope. Representative images were captured and viewed using SPOT 4.1 software running on a G5 Macintosh computer.

Sequence alignments and homology modeling of spirochete MotB proteins. Pair-wise and multiple sequence alignments were produced by MacVector (Cary, NC). Three-dimensional models were predicted by the SWISS-MODEL server (2) using the alignment mode by submitting a pair-wise alignment of the C-terminal domain of MotB from *Helicobacter pylori* with that of an individual spirochete (*T. pallidum* [TP0724], *T. denticola* [TD2765], and *B. burgdorferi* [BB0280]). The Protein Data Bank code for the C-terminal domain of the *H. pylori* MotB bound to *N*-acetylmuramic acid (NAM) is 3CYQ. The molecular viewer program PyMOL (www.pymol.org) was used to generate the structural representations.

RESULTS

General 3D ultrastructure of *T. pallidum*. Thin films containing highly motile *T. pallidum* were plunge-frozen in liquid ethane for CET. Eight treponemes were used for independent 3D reconstructions, one of which was chosen for the surface-rendered model shown in Fig. 1 (see also Movie S1 in the supplemental material for an animation). High-dose single images were analyzed from an additional 168 organisms to supplement the tomographic data. To minimize distortion, images were obtained exclusively from portions of cells that fell across the holes of the support film. Examination of numerous cross-sections also failed to yield discernible evidence for flattening or compression of the cell cylinders as a result of blotting and freezing. As seen in Fig. 1A and throughout, the bacteria retained their characteristic wave-like morphology (58, 64, 82). Side views of tomograms (Fig. 1B) suggested that at least some spirochetes assume a flat-wave configuration, as noted by Sequeira (105), Cox (22), and Peterson et al. (89). Further studies were undertaken to confirm that compression artifacts, which could deleteriously affect subsequent ultrastructural analyses, were not responsible for the flattening as well as to provide basic morphological information that could enhance our interpretation of the CET data and their relationship to *T. pallidum* motility. Examination of live *T. pallidum* by dark-field microscopy (Fig. 2A and B) and by epifluorescence microscopy of motile treponemes labeled with the membrane-selective, styryl dye FM4-64 (123) (Fig. 2C and D) revealed that *T. pallidum* consists of segments of flat waves in different orientations. In these micrographs, one can see that, as has been well described for *B. burgdorferi* (47, 122) and shown for comparison purposes in Fig. 2E and F, segments of treponemes in the plane of focus are sinusoidal, whereas segments perpendicular to the focal plane are linear with a beaded appearance; these are characteristic features of a flat wave (47, 122). The mean ($\pm$ standard deviation) external cell diameter measured from tomographic slices, 200 ± 9 nm, was virtually identical to the value (0.2 μm) typically cited in the literature (68). The mean average diameter of the cytoplasmic cylinders, 145 ± 21 nm, was consistent with measurements of the periplasmic space presented below. Both of these dimensions are considerably less than the corresponding values (approximately 280 nm and 220 nm) for *T. denticola* (60). The radially symmetrical basal bodies (70-nm approximate diameter) assume a slight curvilinear alignment when viewed from the top (Fig. 1A). This arrangement represents an interesting morphological dichotomy from *T. denticola*. *T. denticola* cells typically have two basal bodies at each end; when a third is present, it is off-line from the other two (60).

It was proposed a number of years ago, based on early-generation electron micrographs, that *T. pallidum* harbors an outer coat or slime layer (20), and this putative structure is still invoked to explain virulence properties of the bacterium, particularly its poor surface antigenicity (14, 97). No evidence of an external layer was observed in either longitudinal slices or cross-sections (Fig. 3). Also noteworthy was the absence of the unusual surface structures (i.e., bowls, hook arcades, and tip-associated fibrils) recently described for the termite midgut isolate *Treponema primitia* (Fig. 1 and 3) (80). Although the contours of the OMs generally were smooth, irregularities ranging from small extrusions and outpouchings (Fig. 4A) to large blebs (Fig. 4B) were commonly observed. Readily apparent as well were bulges in the OM where it overlies the basal bodies (Fig. 4C). Previously published micrographs from plastic-embedded ultrathin sections of *T. pallidum* have suggested that the OMs and CMs are in close proximity in regions away

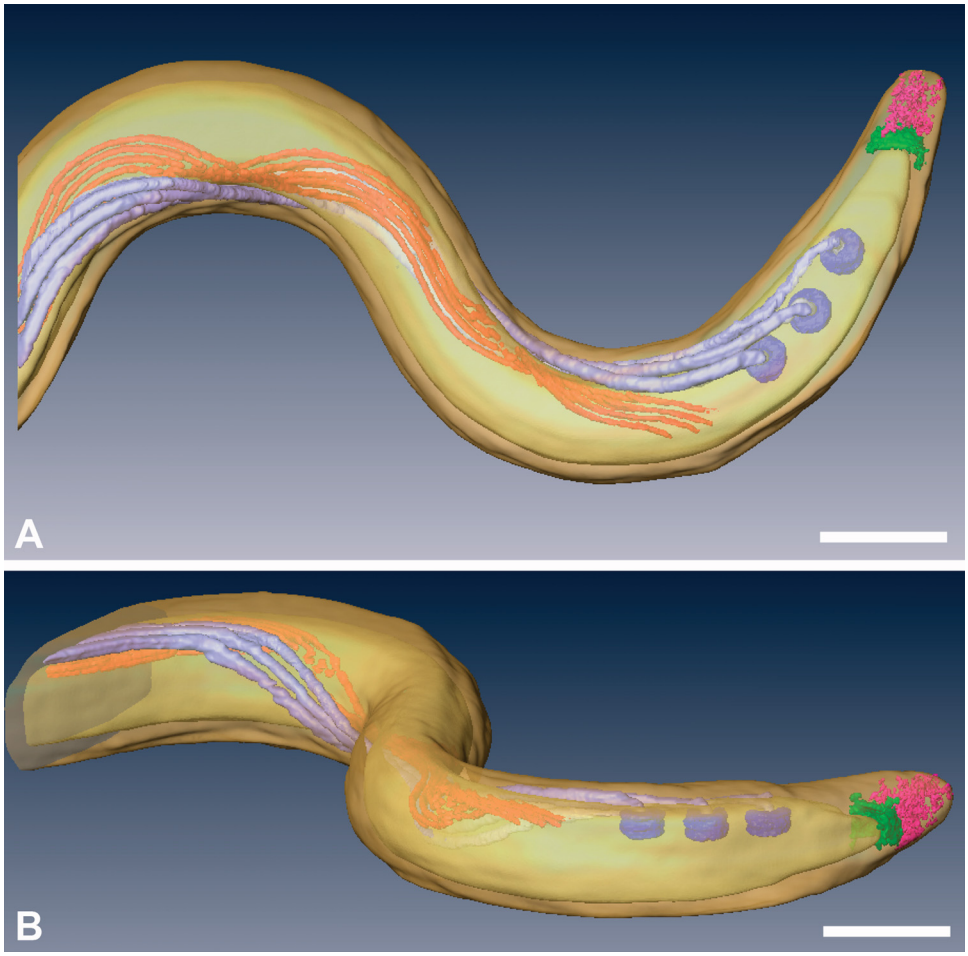

FIG. 1. Top (A) and side (B) views of a surface-rendered model of *T. pallidum*, showing the outer and cytoplasmic membranes (transparent yellow), basal bodies (dark lavendar), flagellar filaments (light lavendar), cytoplasmic filaments (orange), cap (green), and cone (pink). The peptidoglycan layer was not rendered. Also see Movie S1 in the supplemental material for animation. Bars, 200 nm.

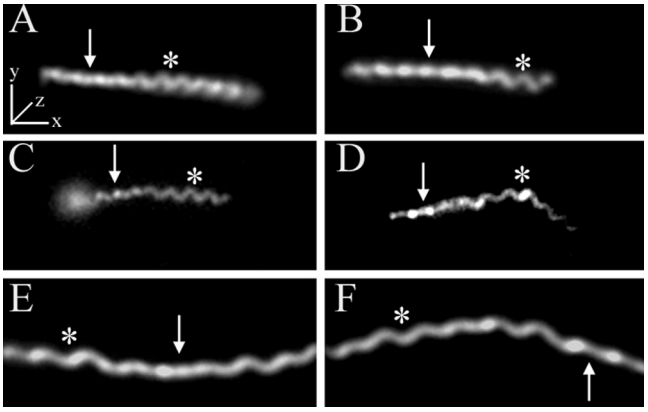

FIG. 2. *T. palladium* has a flat-wave morphology. Representative micrographs show the flat-wave morphology of *T. pallidum* as revealed by dark-field microscopy (A and B) and by epifluorescence microscopy (C and D) following labeling of motile treponemes with FM4-64. Panels C and D show sequential images of the same treponeme; note how the leftward segment changes from helical to linear as it moves away from the focal plane. (E and F) For comparison purposes, dark-field images of a *B. burgdorferi* 297 cell in two different orientations are shown. Arrows and asterisks indicate regions of the spirochetes that are parallel to the *z* axis or in the *x-y* plane, respectively. Bars, 5 μm.

from the periplasmic flagella but widely separated by the flagellar filaments (58, 82). Longitudinal slices and cross-sections demonstrated, instead, that the two bilayers are well separated along the entire length of the spirochete, gradually widening to accommodate the flagellar filaments (Fig. 1 and 3). The mean distances between the midpoints of the two membranes in regions without and with flagella, 28 ± 2 nm and 48 ± 4 nm, respectively, yielded values for the periplasmic space of approximately 20 and 40 nm. Once away from the basal bodies, the flagella typically do not abut the inner leaflet of the OM but are separated from it by a thin layer of periplasm (Fig. 3). The mean diameter of the flagellar filaments (17.34 ± 0.77 nm) is slightly smaller than those recently determined for *T. denticola* (18 to 20 nm) (60) and *T. primitia* (20 nm) (80). As in *T. denticola*, the filaments are separated from each other by a uniform translucent space approximately half the diameter of the filament (9.7 ± 1.2 nm) (Fig. 1B and 3D). Interestingly, in many sections it was evident that the periplasmic space is not homogeneous and that the electron density in the vicinity of the CM typically is greater than near the OM (Fig. 3A). A structurally complex cell end, described in detail below, also was readily discernible (Fig. 1 and 3B).

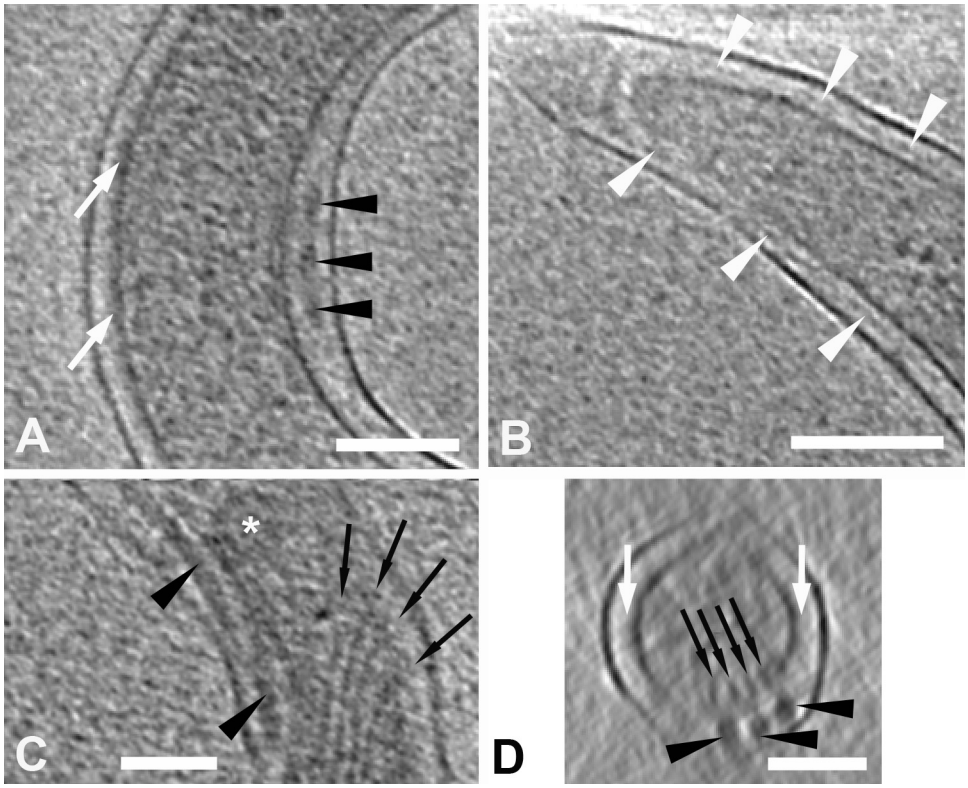

FIG. 3. General 3D ultrastructure of *T. pallidum*. Slices, 1.8-nm thick, are from the tomogram represented by the model in Fig. 1. Black arrowheads, periplasmic flagella; white arrowheads, peptidoglycan; black arrows, cytoplasmic filaments; white arrows, increased density in the periplasm adjacent to the cell membrane; asterisk, basal body. (A) Widening of the periplasmic space to accommodate the flagellum. (B) The peptidoglycan layer is typically well-visualized near the cell end. (C) Attachment of the cytoplasmic filaments to the cytoplasmic membrane opposite the basal bodies; note the convergence of the filaments as they leave their sites of attachments (also compare with Fig. 1 and movie S1 in the supplemental material). (D) Cross-section showing the positioning of the cytoplasmic and flagellar filaments on opposite sides of the cytoplasmic membrane. Bars, 100 nm.

Distinctive structural components of some spirochetes, including treponemes, are the intermediate-like filaments, composed of highly conserved 83-kDa CfpA monomers that wind around the cell cylinder along the inner surface of the CM (60–62, 124). Insertional inactivation of the *cfpA* gene in *T. denticola* revealed that the filaments function to maintain chromosome organization and foster normal cell division (63). Between four and six cytoplasmic filaments were visualized in each of the tomographic reconstructions. As noted for *T. denticola* (60), the cytoplasmic filaments converged from their attachment points opposite the basal bodies to form tight, but nontouching, arrays that run roughly parallel to the flagellar filaments along the inner wall of the CM (Fig. 1 and 3C). We were unable to discern distinct structures where the filaments insert into the CM.

Complexity and diversity of cell end attachment structures. Studies from the 1970s using cultured cells reported that *T. pallidum* attaches end-on to mammalian cells (40, 52, 89). We began our ultrastructural examination of the *T. pallidum* tip by reassessing its function and contribution to cytoadherence. Treponemes freshly harvested from rabbit testes were incubated for 3 h with partially confluent monolayers of rabbit cottontail Sf1Ep cells (spirochete-to-cell ratio of 10:1), a cell line known to support replication of organisms and retention of high degrees of virulence in vitro (23). In three independent experiments, an average of 3.20% ± 0.4% of the input treponemes remained attached stably to the epithelial cells (i.e., they were not removed by extensive washing). This percentage is in line with earlier studies which examined the attachment of treponemes to a variety of mammalian cell lines and fibronectin (41, 52, 89, 113). The overwhelming majority (approximately 90%) of the adherent treponemes were attached at one or both ends, while a surprisingly high percentage (33.46 ± 3.46%) was anchored at both (Fig. 5); attached spirochetes were vigorously motile.

Compared with the other spirochetes examined thus far by CET, *T. pallidum* tips displayed greater structural complexity. They also exhibited an unexpected degree of structural diversity, with at least four distinguishable morphotypes observed in each of two independently prepared samples (Fig. 6). Type 1 ends (Fig. 3B and 6A), the simplest, consisted of a crescent-shaped cap near the rounded terminus of the CM followed by a porous-appearing cone. Thin fibrils often were observed extending from the cones to the OM (Fig. 6A); cross-sections (Fig. 6A, inset) confirmed that the fibrils emanated circumferentially from the cones. Type 2 ends (Fig. 6B) contained a vesicle in front of the CM; the density of the material within the vesicle was similar to that of the cytoplasm. In some organisms the vesicle was free-standing in a "clear zone" within the periplasmic space, whereas in others it was connected to

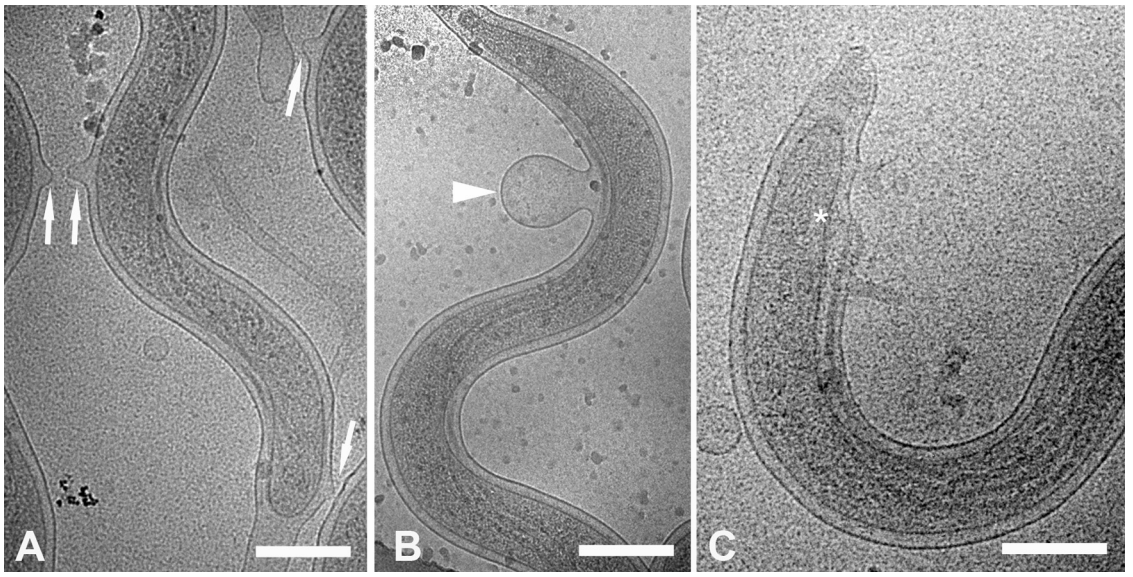

FIG. 4. Fluidity of the *T. pallidum* OM. Cryo-electron micrographs show OM extrusions (arrows) (A), OM blebs (arrowhead) (B), and the bulge in the OM over a basal body (asterisk) (C). Bars, 200 nm.

the rounded terminus of the CM by a stalk or membranous extension; distal to these structures was the cone with fibrils. Type 3 ends (Fig. 6C) resembled the type 2 morphotype, except that they possessed either tapering or bulbous extensions of periplasm beyond the cone. In some type 3 ends, deformation of the cone also was evident (Fig. 6C). Type 4 ends, the most bizarre, resembled type 3 ends except that their extended tips contained one or more vesicles with material of lower density than the cytoplasm (Fig. 6D). From the 176 cells observed, 214 ends could be categorized; 83 were type 1, 70 were type 2, 41 were type 3, and 20 were type 4 (Table 1). Among the 176 cells, there were 38 for which both ends could be typed (Table 1). Of these, only 13 had ends of the same type, while one-half (19) had at least one type 1 or type 2 tip. No cells with only type 4 ends were found.

An important question is whether the pleomorphism of the cell ends is artifactual, possibly caused by trauma at the time of extraction from the rabbit testes, or is a product of the syphilis spirochete's poorly understood membrane biology. Two sets of observations argue for the latter. Figure 7A and B show two treponemes in different stages of cell division. In Fig. 7A newly formed cytoplasmic cylinders flank a rounded, nascent cone; this dividing cell appears to be generating type 1 ends. The spirochete in a later stage of division (Fig. 7B) contains an elongated "tube" of OM joining daughter cylinders with distended cones and may be generating type 3 ends. We also noted that, in addition to blebs derived from OMs, treponemes generate a second class of blebs with both outer and CMs; envelope-derived blebs near cell ends were common (Fig. 7C and D). Figure 7C shows a striking image of a bacterium with an envelope-derived bleb very similar in appearance to the vesicle in its type 4 end.

Localization of peptidoglycan within the periplasmic space and relationship to the motility apparatus. A number of years ago, we demonstrated the presence of PG in *T. pallidum* by EM and biochemical analysis of sacculi obtained following extensive detergent extraction and protease treatment of whole treponemes (98). CET enabled precise localization of

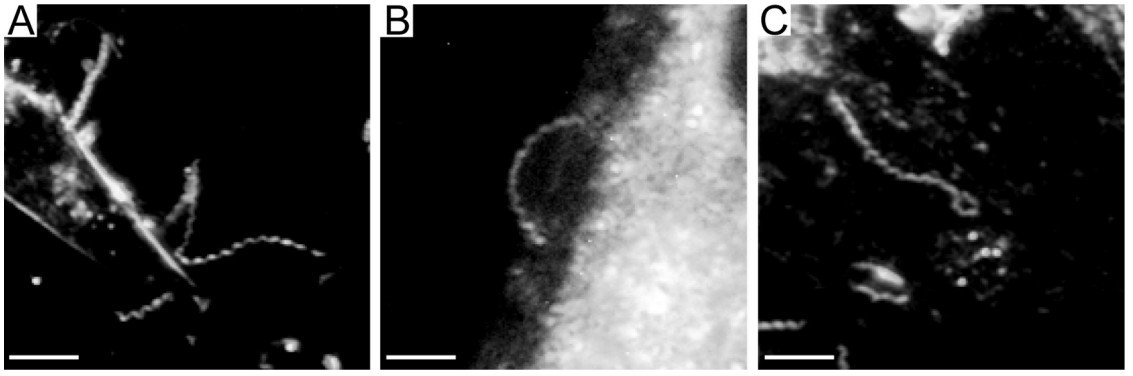

FIG. 5. *T. pallidum* stably attaches to rabbit epithelial cells predominantly via its tip. Suspensions of treponemes freshly extracted from rabbit testes were incubated for 3 h with rabbit cottontail Sf1ep cells at a spirochete/cell ratio of 10:1. Micrographs show treponemes attached by one tip (A), by both tips (B), or along the cell cylinder (C). Bars, 10 μm.

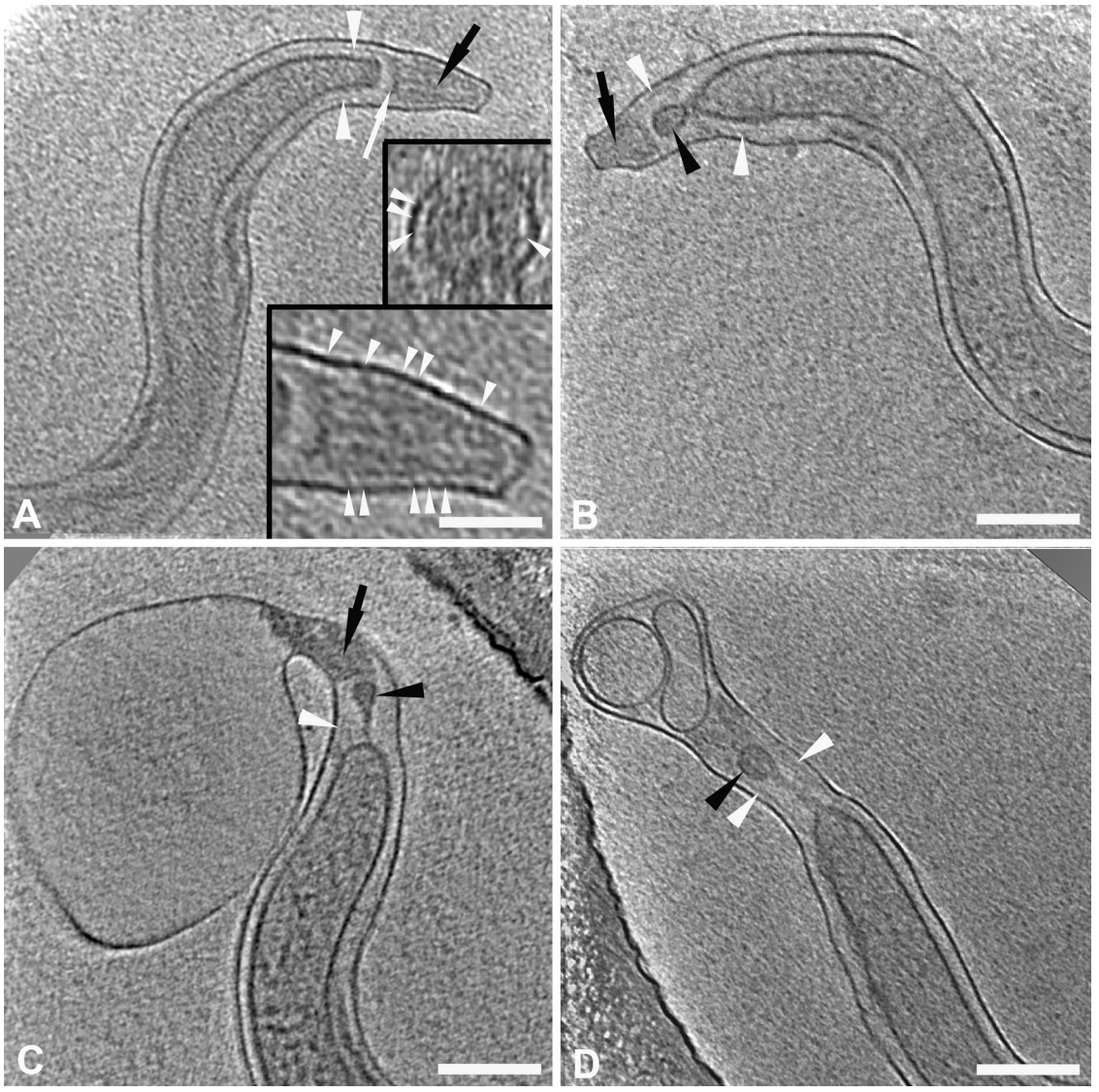

FIG. 6. Ultrastructural complexity and diversity of *T. pallidum* cell ends. Slices 1.8 nm thick are from cryo-tomograms of *T. pallidum* and show cell end morphotypes 1 to 4 (A to D, respectively). White arrowheads, peptidoglycan; black arrowheads, "vesicles"; black arrows, "cones"; white arrow, "cap." In both the cross-section and longitudinal section presented in the insets in panel A, the arrowheads indicate the fine fibers between the cone and the outer membrane. Note that the PG extends up to the cap in panel A. In panels B to D, note that the vesicle seems to be tethered to the cytoplasmic cylinder and that the peptidoglycan extends well past the end of the cytoplasmic cylinder. Bars, 200 nm (100 nm in inset).

this material and evaluation of its relationships to other periplasmic constituents. The PG was identified as a thin line of intermediate density between the OM and CM. In regions without flagellar filaments, it was approximately midway within the periplasmic space, while in regions containing flagella it was beneath the filaments (Fig. 8A and B). Intensity plots (Fig. 8C and E) confirmed these relationships, demonstrating as well the greater density of the periplasm on the CM side of the PG. Also noteworthy was that the distance between the CM and PG in sections containing flagella was slightly less than in sections without flagellar filaments (12 ± 2 nm versus 15 ± 2 nm, respectively) (see also the intensity plot in Fig. 8C), suggesting that the flagellar filaments locally compress the PG layer. Examination of single cryo-EM images and washed, negatively stained treponemes provided additional evidence that the flagella overlie the PG. Figure S1A in the supplemental material shows a bacterium with a large protrusion of flagella surrounded by OM analogous to those described by Charon et al. (17, 47) for *Treponema phagedenis*, *T. denticola*, and *B. burgdorferi*. Figure S1B in the supplemental material, which is comparable to numerous electron micrographs of disrupted treponemes published over the years, shows a negatively stained organism without an OM and in which the flagella are in disarray alongside the cytoplasmic cylinder. Neither image is consistent with the flagellar filaments lying beneath a relatively rigid meshwork of PG.

In contrast to the mid-cell regions, where PG was often difficult to discern, near the cell ends it was well visualized within the periplasmic space, clearly extending beyond the CM (Fig. 3B and 6). Whether it extends all the way to the cell tips,

TABLE 1. Distribution of cell ends by type[a]

Basis of analysis (*n*)	No. of cell ends with indicated morphotype				
	Type 1	Type 2	Type 3	Type 4	Total
All cell ends (214)					
Tomogram	3	2	2	1	8
Cryo-TEM	80	68	39	19	206
Total	83	70	41	20	214
Ends in cells with two typeable ends (38)					
Type 1	5	7	1	1	14
Type 2		7	8	1	16
Type 3			1	7	8
Type 4				0	0
Total	5	14	10	9	38

[a] Data are combined results from two independently prepared samples involving a total of 176 treponemes: 130 cells with only one cell end observed, 38 cells with both cell ends (all observed by cryo-electron microscopy), and eight tomograms.

however, could not be determined with certainty. In some tomograms and single images of cells with type 1 or type 2 ends, the PG appeared to merge with the cap (Fig. 3B and 6A). In others, however, it appeared to outline the cap and cone (Fig. 6B). Examination of negatively stained treponemes lacking OM suggested that the PG layer does indeed completely follow the contour of the OM. Figure S2 in the supplemental material shows one such organism with a type 2 end in which the murein sacculus appears to extend to the tip of the bacterium, enclosing a vesicle and cone.

The currently accepted model for spirochetal motility holds that interactions between PG and MotB stabilize the stator (MotA/MotB) complex within the CM, providing a stationary platform against which the rotor and rod rotate to generate torque (16, 72, 79, 80). Upon close inspection of slices near the cell ends of *T. pallidum*, we noted a number of instances in which PG could be observed extending between basal bodies (Fig. 8B and data not shown). The section in Fig. 8D, along with the corresponding intensity plot in Fig. 8E, delineate particularly well the rod, hook, and flagellar filament extending nearly vertically to protrude against the OM, while the PG layer underneath the filament intersects the basal body. Using *T. primitia* and *B. burgdorferi* high-resolution models as guides (72, 79), it was determined that the PG contacts the superior aspect of the stator. To confirm this assignment, we modeled the flagellar motors by mutually aligning and averaging three easily identifiable basal bodies (Fig. 8F) followed by cylindrical averaging about axes defined by the rods. The resulting cylindrical average had a resolution of approximately 10 nm, sufficient to identify the rod, rotor, export apparatus, stator, C-ring, and P-collar components of the flagellar motors (Fig. 7G) (72, 79). The cylindrical average then was used to determine the location and orientation of the basal bodies in the CM via correlation alignment. This analysis positioned the stator squarely within the membrane, localizing the PG-basal body

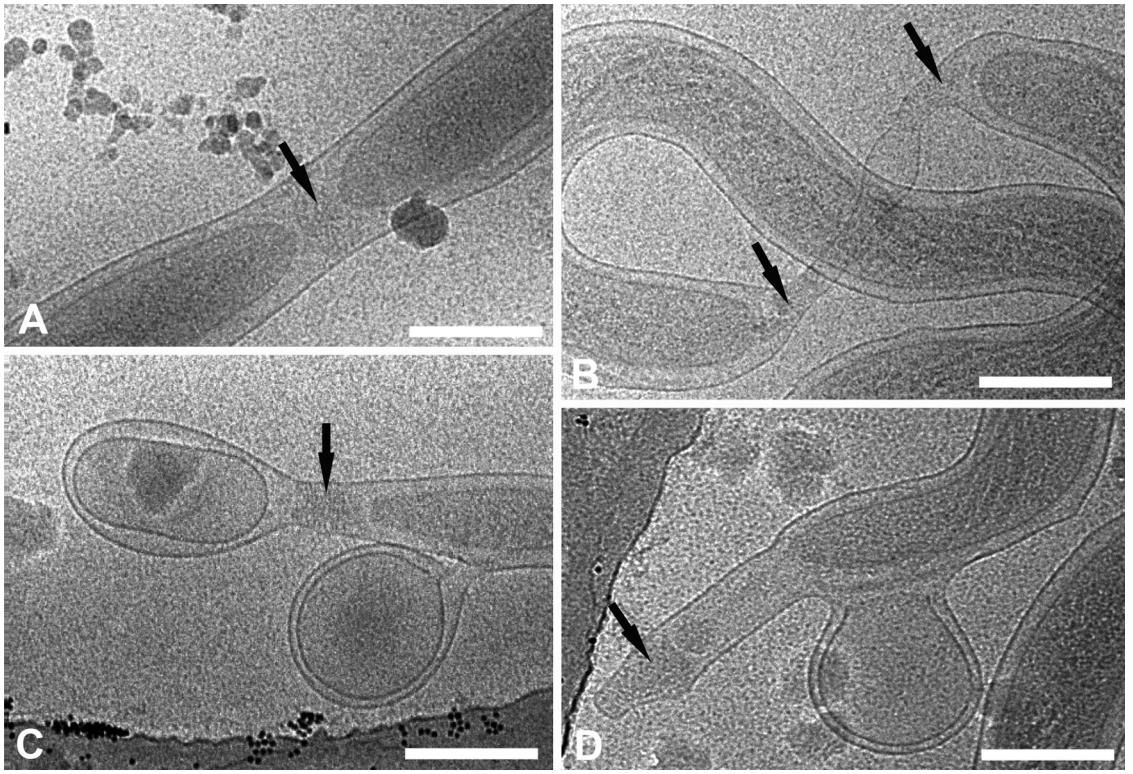

FIG. 7. Events during cell division and the generation of cell envelope-derived blebs may help to explain the pleomorphism of *T. pallidum* ends. (A and B) Cryo-electron micrographs of early (A) and late (B) stages of division show nascent cone formation (black arrows). (C and D) Treponemes are shedding cell envelope-derived blebs which retain both outer and cytoplasmic membranes. Splotches are frost contamination. Bars, 200 nm.

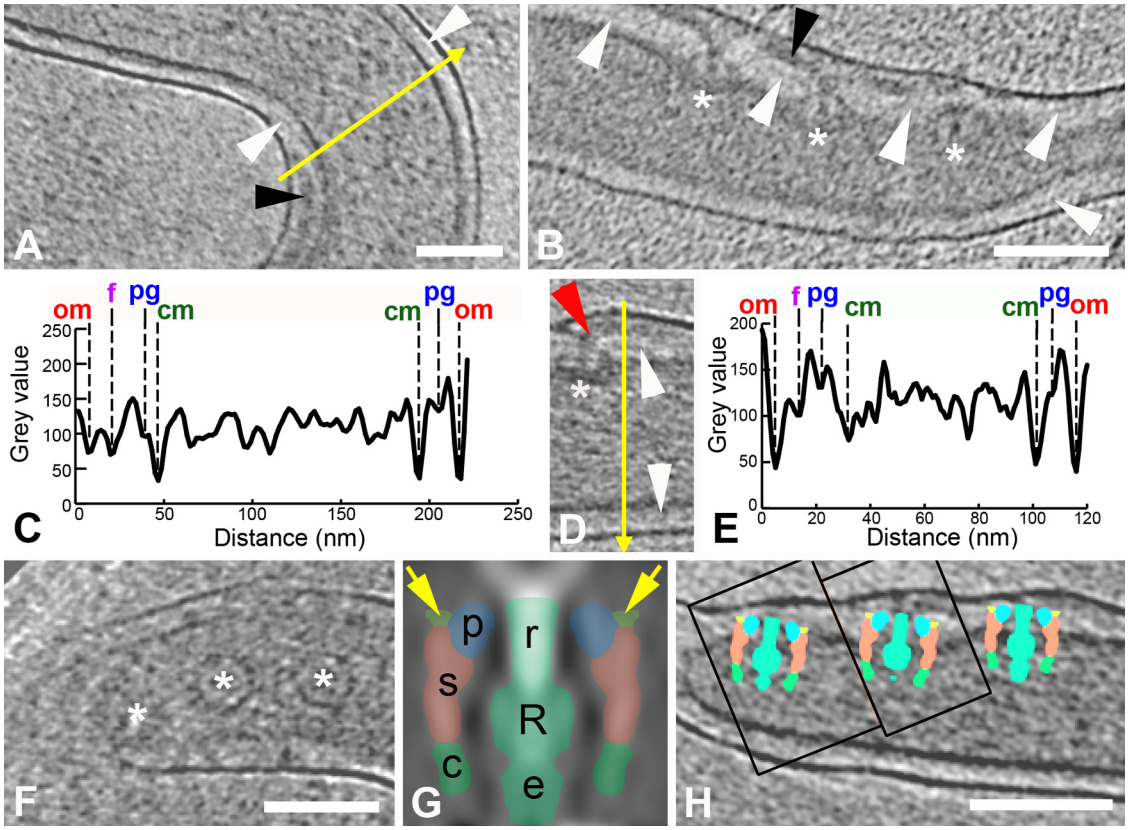

FIG. 8. Spatial relationships of PG within the periplasmic space. White arrowhead, PG; black arrowhead, flagellar filament; red arrowhead, hook; asterisk, basal bodies. In panels A, B, and D, slices 1.8 nm thick are from different tomograms. (A) The location of the PG between the flagellum and the cytoplasmic membrane; an intensity profile along the direction of the yellow arrow is shown in panel C. (B and D) The PG appears to attach near the P-collar and stator of the basal body. Note that the hook is clearly seen in panel D. An intensity profile along the direction of the yellow arrow in panel D is shown in panel E. Abbreviations used in the intensity plots in panels C and E: om, outer membrane; f, periplasmic flagellum; pg, peptidoglycan; cm, cytoplasmic membrane. (F and H) Slices 10 nm thick, both from the same tomogram, showing the three basal bodies that were cut out as subvolumes, aligned with each other, and rotationally averaged in 3D to create the low-resolution model shown in panel G. (G) A central section of the model is interpreted according to the methods described by Murphy et al. (79) as follows: r, rod; R, rotor; s, stator; p, P-collar; c, C-ring; e, export complex. The light green areas (also indicated by yellow arrows) depict the sites of PG binding at the boundaries between the P-collar and the stator. (H) Central slices from the tomographic subvolumes containing the left two basal bodies (boxes) were inserted into the central tomographic slice containing the right-most basal body; the corresponding section from the model in panel G was then superimposed on each basal body to create the final composite image. Bars, 100 nm (the scale of panel D is the same as that in panel B).

site of interaction near the boundary between the P-collar and stator (Fig. 8H).

Whereas mutagenesis could be used to confirm the above results with most bacterial pathogens, a genetic approach is not yet possible with *T. pallidum*. We reasoned, however, that secondary structure analysis in conjunction with protein structural modeling could provide indirect evidence for a possible interaction between PG and MotB in *T. pallidum*. As shown in Fig. 9A, *T. pallidum* MotB aligns well with the Mot B proteins of *E. coli* and *H. pylori* and contains at its N terminus a predicted transmembrane-spanning α-helix and at its C terminus a $LSX_2RAX_2VX_3L$ motif, which is conserved throughout the family of OM protein A-like PG binding domains (32); these similarities predict that *T. pallidum* MotB is a cytoplasmic membrane protein with topology similar to its well-characterized orthologs. In close proximity to the $LSX_2RAX_2VX_3L$ motif, there are two regions of low sequence conservation that have been shown by X-ray crystallographic studies of the *H. pylori* MotB to form loops, which are important structurally for binding of PG (101). The alignment also reveals that *T. pallidum* MotB contains many of the residues shown by Blair et al. (7) in a mutagenesis screen to result in complete or partial loss of motility in *E. coli*. To further assess the likelihood that *T. pallidum* MotB interacts with PG, the protein was modeled by homology to the solved crystal structure of the PG binding domain of *H. pylori* MotB complexed with NAM (101). The structure predicted (Fig. 9B) for the C terminus of *T. pallidum* MotB closely resembles that of the *H. pylori* MotB. Additional analyses comparing the modeled PG binding loops of the *T. pallidum* MotB to those of the *H. pylori* MotB suggest that, despite the degree of sequence heterogeneity, the PG-protein interactions, which have been shown to be mediated largely by main-chain atoms, are conserved at the structural level (101). Comparable alignments (Fig. 9A) and structural predictions (Fig. 9B) were obtained for the MotB proteins of *T. denticola* and *B. burgdorferi*.

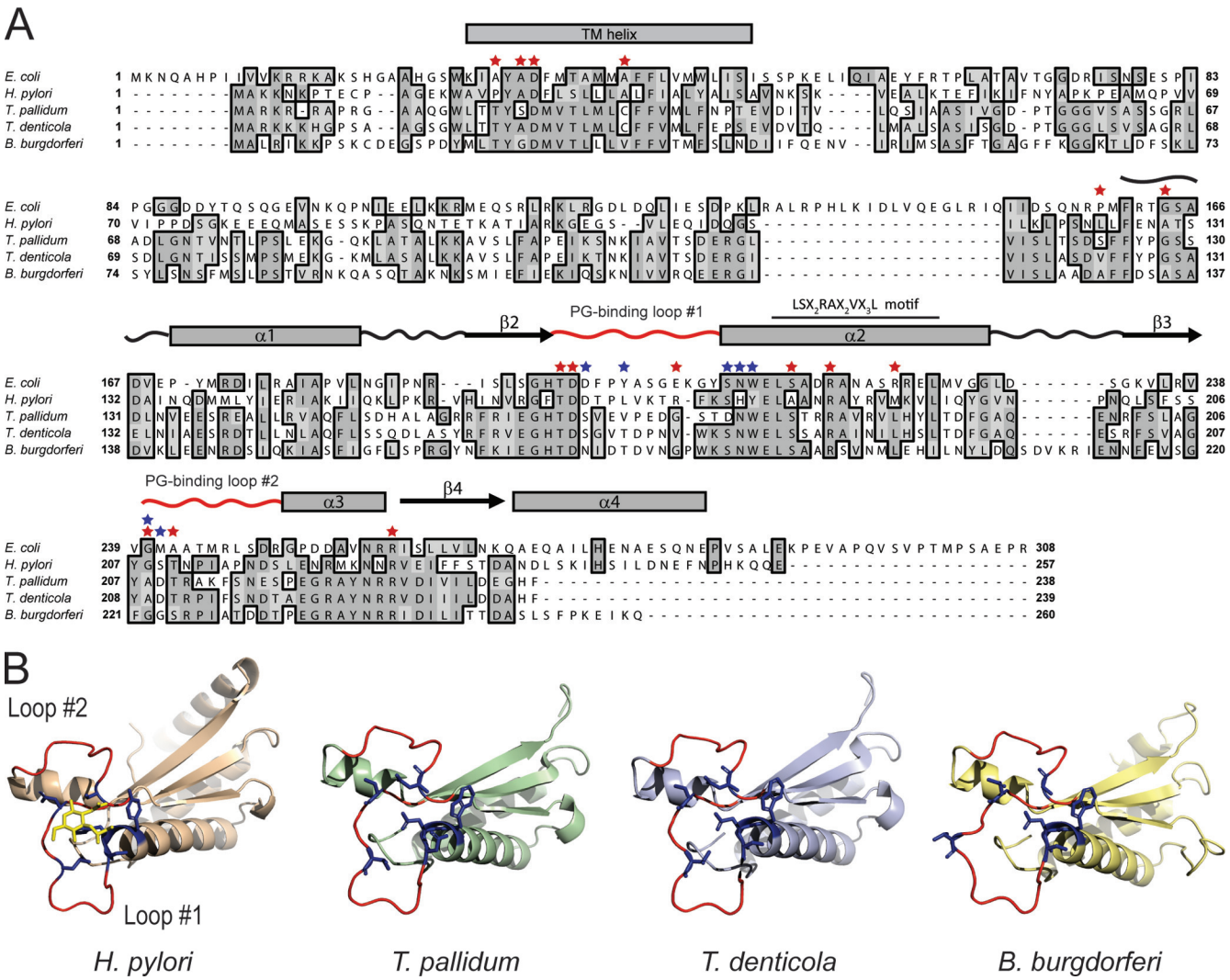

FIG. 9. Conservation of functional residues, membrane topology, and PG binding domains in spirochete and gram-negative MotB proteins. (A) Sequence alignment of MotB proteins. Dark and light gray shading indicate identical and similar amino acids, respectively. The predicted single α-helical transmembrane domains of the spirochete MotBs, based on topological analysis of *E. coli* MotB (21), are designated. A line overscores the $LSX_2RAX_2VX_3L$ motif. Residues that were shown by Blair et al. (7) in a mutagenesis screen of MotB to result in complete or partial loss of motility in *E.* coli are indicated by red stars. Amino acids that form the NAM binding site are shown by blue stars (101). Curvy lines, rectangles, and arrows represent sequences that fold into loops, α-helices, and β-sheets, respectively, as determined by X-ray crystallography of the *H. pylori* MotB PG binding domain (101). The curvy lines, representing PG binding loops 1 and 2, are red. (B) Structure of the PG binding domain of the *H. pylori* MotB bound to NAM (yellow) and three-dimensional models (see Materials and Methods) of the corresponding regions from different spirochetes. The vantage point of all structural representations consists of looking down into the PG binding groove formed by PG binding loops 1 and 2 (red). The NAM binding residues are shown as sticks and are blue.

DISCUSSION

CET has emerged as a robust technology for 3D imaging at near-molecular dimensions under conditions that preserve cells and organelles in a close-to-native state (70, 71). Spirochetes are excellent candidates for CET because they possess a richness of structural detail (55, 61) and are so thin that they do not require sectioning or milling following vitreous freezing of thin films in order to be imaged in their entirety. Sequencing of ribosomal DNA genes and subsequently whole genomes has established that spirochetes comprise a unified, though deeply branching, eubacterial phylum (86). CET has enhanced the ability of investigators to identify structural commonalities among this ancient group of organisms while, at the same time, calling attention to features which enable individual species to meet the divergent evolutionary demands imposed by pathogenic lifestyles or residence in unusual microenvironments. For *T. pallidum*, it has the potential to provide ultrastructural information needed to resolve long-standing dilemmas of physiology and host-pathogen interactions that are further complicated by the bacterium's minimalist genome, unusual OM molecular architecture, and recalcitrance to continuous in vitro cultivation (68, 83, 96).

Because of their double-membrane ultrastructure, *Borrelia* spp. and treponemes often are likened to gram-negative bacteria. The inaccuracy of this analogy was recognized well before the publication of genomic sequences. Freeze-fracture

electron microscopy demonstrated that borrelial and treponemal OMs contain a much lower density of integral membrane proteins than do those of gram-negative bacteria (9, 12, 94, 117, 118), while biochemical analysis revealed that they lack lipopolysaccharide (5, 111). Because lipoproteins do not form particles in freeze-fractured membranes (65), this technique underestimates the total amount of protein associated with membranes that have a high content of lipoproteins. Consequently, investigators have had to rely upon immunolocalization methodologies to assess the relative amounts of lipoproteins on the surface of pathogenic spirochetes. A major difference between *B. burgdorferi* and *T. pallidum* revealed by these investigations relates to the location of their lipoproteins. *B. burgdorferi* (and other borrelial species) tethers numerous lipoproteins to its surface, whereas, with one possible exception (11), all lipoproteins studied in *T. pallidum* are periplasmic, associated either with its CM or the inner leaflet of the OM (14, 97, 115). To date, only one lipoprotein, an OppA homolog, has been reported to be surface exposed in *T. denticola* (39). The phylogenetic implication of these findings is that *Borrelia* spp. possess a mechanism, though still poorly defined (24, 104), for efficient surface localization of lipoproteins which is not present in treponemes. CET has provided support for this dichotomy. Kudryashev et al. (66) reported that *B. burgdorferi* and other Lyme disease spirochetes possess a linear structure external to the OM, which they designated a slime layer and attributed to surface-adherent proteins from the medium. Liu and coworkers (72) confirmed the existence of a surface layer on *B. burgdorferi* but, based on the results of proteinase K digestion, concluded more plausibly that it consists of lipoproteins on the borrelial surface. In contrast to *B. burgdorferi*, and consistent with the much lower density of outer lipoproteins in treponemes, CET did not identify a comparable surface layer on *T. primitia* (80), *T. denticola* (60), or *T. pallidum*. Our current findings corroborate earlier studies attributing the poor antigenicity of intact *T. pallidum* to its OM architecture (14, 26, 97).

T. pallidum represents an extreme among spirochetes with respect to the remarkably low protein content of its OM (14, 97). The physiologic conundrum raised by this unusual OM architecture is how sufficient nutrients traverse the bilayer to sustain the bacterium's metabolic activities (93). Adding to this enigma is the genomic sequence, which failed to identify orthologs for gram-negative porins (14, 44, 82). Conventional ultrathin sections of *T. pallidum* have depicted the OM and CM as often juxtaposed in regions away from the flagella (58, 82). Such a topological arrangement potentially would facilitate the delivery of nutrients traversing the OM to the relatively abundant transporters associated with the CM. CET, however, has provided compelling evidence that the putative contact points between the two membranes are an artifact of the preparation process for plastic embedding and that, except where widened to accommodate the flagella, they are separated by a relatively uniform distance comparable to that in cultivatable spirochetes and even *E. coli* (18, 54, 60). It seems implausible, therefore, in light of these findings, that the syphilis spirochete can entirely forego the need for conventional, fixed channels. Indirectly supporting the existence of as-yet-unidentified porin-like proteins in the *T. pallidum* OM is TP0326 (Tp92) (15), an ortholog for BamA (β-*b*arrel *a*ssembly *m*achinery; Omp85/YaeT) (D. C. Desrosiers and J. D. Radolf, unpublished observations), an essential, highly conserved OM protein in gram-negative bacteria responsible for the insertion of β-barrel proteins into the OM (46, 103). The discovery of pore-forming OM proteins in *Borrelia* that are phylogenetically unrelated to gram-negative porins (90, 112) further supports this line of thinking.

Whereas the OMs of gram-negative bacteria are highly resistant to physical disruption and detergent solubilization (81), those of spirochetes are labile and hypersensitive to detergents (12, 14, 95). The relationship between the respective OMs and the PG layer is a major determinant of their physical properties. In gram-negative cells, the PG is closely apposed to the OM (54, 75) and tightly linked to it both covalently, via Braun's lipoprotein, and noncovalently via interactions with lipoproteins, such as peptidoglycan-associated lipoprotein, and numerous membrane-spanning proteins, most notably, porins and OmpA (32, 81, 85). Spirochete OMs, on the other hand, have no demonstrated biochemical linkage with PG and, as has been shown by various fractionation techniques (8, 14, 100, 108), are easily separated from cell cylinders, arguing against the existence of extensive noncovalent interactions between PG and OMs. The irregularities and extrusions of the OM in *T. pallidum* and the propensity of *T. pallidum* and *B. burgdorferi* to shed OM blebs (9, 18, 66, 94) is further evidence that OMs of spirochetes are, at most, loosely tethered to underlying cell envelope constituents. While shedding OMs blebs by *T. pallidum* has not received extensive attention in the past, we have demonstrated by freeze-fracture EM unequivocal OM blebs on syphilis spirochetes (9). Like CET, freeze-fracture employs plunge-freezing of samples but does not involve comparable sheer forces created by blotting, arguing that the OM blebs observed in the present study were not caused during sample preparation.

Based on conventional EM, it has long been believed that the PG in spirochetes is juxtaposed to the CM (26, 55, 58). The analysis of tomograms has demonstrated, however, that this conception is almost certainly the result of an artifact of specimen preparation and that the PG actually resides within the periplasmic space (60, 66, 72, 79). This information, coupled with the demonstration herein of a difference in electron density of material on opposite sides of the PG, enables us to propose that the periplasmic space of most spirochetes (*T. primitia* possibly being an exception [see below]) consists of two functionally distinct compartments or zones, as opposed to the homogeneous periplasmic compartment of gram-negatives (54, 75). The putative zone below the PG contains the periplasmic domains of relatively tightly packed integral membrane proteins (9, 94) and the polypeptide moieties of lipoproteins, many of which are substrate binding proteins for CM-associated ABC permeases (29–31, 33, 43, 44, 48, 119). The less-dense zone external to the PG is postulated to contain soluble polypeptides (e.g., chaperones, antioxidant enzymes) (78, 107), the protein moieties of a presumably small number of lipoproteins anchored to the inner leaflet of the OM (53), and the periplasmic domains of mostly unidentified OM-spanning proteins (9, 12, 49, 50, 94, 99, 117, 118). The postulated outer zone also contains the motility apparatus. CET has been used to clearly visualize the expansion of this compartment in the vicinity of the flagellar motor and in regions of the cylinder

containing flagellar filaments (18, 60, 66, 80). Our proposed organization of the periplasmic space requires some type of a scaffold to maintain the PG at a fixed distance from both membranes. Interactions of the PG matrix with proteins within the lower zone could provide much of the supportive framework, while MotB would provide anchorage at the cell ends. In *T. pallidum*, TP0292 (Tpn50), the only exported protein with a recognizable peptidoglycan binding motif (25, 51), could further stabilize the PG along the length of the cylinder.

Elucidation of the complex biophysics of spirochete motility requires an understanding of the physical and spatial relationships between the flagellum and the cell envelope. In accord with the findings of Liu et al. (72) for *B. burgdorferi*, we visualized flagellar filaments above the PG in multiple longitudinal and cross-sections, and we confirmed this observation by imaging flagella separated from the cytoplasmic cylinders in "washed" treponemes and as protruded filaments. We also noted that the PG is closer to the CM in regions with flagella, suggesting that the filaments are compressing the murein layer. In their examination of *T. primitia*, Murphy and coworkers (80) described inner and outer periplasmic layers which contained the flagellar filaments, and they designated the lower channel to be PG, based on its presumed interaction with MotB. They proposed a model for spirochete motility in which the flagella, rotating within a channel created by the two layers, can transmit rotational energy to either layer. This model, however, cannot apply to the other spirochetes examined by CET, all of which lack an upper periplasmic layer. Instead, we propose that in these organisms, the flagella rotate against the PG without translating about the circumference of the cell cylinder and that the deformations of the cell cylinder that drive motility are always a result of this rotation. Whether the spirochete assumes a flat-wave or a spiral configuration depends on physical parameters, primarily the stiffness of the flagellum relative to the cell body (19, 35). These parameters must be different for *T. denticola* and *T. pallidum*, given that *T. denticola* lacking flagella are helical (102), whereas the shape of *T. pallidum* most closely resembles a flat wave, as reported earlier by several groups (22, 89, 105).

The energy-generating unit of the flagellar motor, the stator, must be immobilized within the CM in order to produce torque. In gram-negative bacteria, this is accomplished by the binding of the radially arranged MotB subunits to the PG layer near the OM. While our data set did have a different level of resolution for imaging the motor compared to those published for *T. primitia* (79) and *B. burgdorferi* (67, 72), we were able to identify the components of the motor identified in these earlier studies and assess their interactions with PG. Our analysis indicates that the PG intersects the basal body at or near where the top of the stator meets the neighboring structure called the P-collar, the site predicted by Murphy et al. (79) from their modeling of *T. primitia*. We complemented our CET data by using bioinformatics and homology modeling to better understand the potential interactions between the stator (i.e., MotB) and PG. We found that the MotB proteins of *T. pallidum*, *B. burgdorferi*, and *T. denticola* have predicted membrane topologies and PG binding sites highly similar to those of their gram-negative stator orthologs, providing indirect support for our CET modeling analysis and suggesting that a MotB-PG interaction may occur in other spirochetes. Recently, Kudryashev et al. (67) reported for *B. burgdorferi* that PG binds to the P-collar. The lack of knowledge of the P-collar content and the relative position of MotB amino acids relative to that structure create an open question that requires further investigation at the molecular level. In any event, it is noteworthy that the PG was visualized more readily near the cell ends, suggesting that it is thicker and/or more highly cross-linked in a presumed stress-bearing region of the cell wall but thinner elsewhere, as required for the cell cylinder to be flexible (19). The general thinness of the PG suggests that it is predominantly, perhaps exclusively, a single layer in *T. pallidum*, as it is in gram-negative cells (45, 116).

Attachment of spirochetes to cells and extracellular matrix at sites of inoculation in skin and mucosa is widely considered to be the critical initial step of syphilitic infection (14, 68). The sequence of events during attachment of treponemes is poorly understood, and our experiments do not preclude the possibility that *T. pallidum* utilizes receptors along its length to establish an initial "foothold" at the site of inoculation and elsewhere during dissemination (14). Our results, however, are in agreement with earlier reports that the tip structure is involved in stable attachment to eukaryotic cells (40, 52, 89), and they suggest the intriguing possibility that treponemes anchored to cells or matrix via this structure in vivo may be less predisposed to early dissemination than their unattached counterparts (97). Early electron microscopy studies called attention to the unusual morphology and anatomical diversity of *T. pallidum* tips (58, 84, 120). In retrospect, these investigations were harbingers of the extraordinary pleomorphism of cell ends revealed by CET. While the extraction of *T. pallidum* from the testis is believed to be a relatively gentle procedure, it is certainly conceivable that physical stress on adherent organisms during harvesting could be a contributory factor to cell end polymorphisms. Indeed, more studies along these lines are clearly indicated, as is the development of methodologies to assess the attachment competence of the different cell end morphotypes. On the other hand, observations from two different phenomena serve as proof of principle for the contention that generation of cell end polymorphisms also may have roots in the syphilis spirochete's complex membrane biology. The first is cell division, an intricate sequence of events during which a cell cylinder is severed at the site of formation of the FtsZ ring concomitant with the positioning and insertion of new flagellar basal bodies into the CMs of the future daughter cells near the septation site; after closure of the cytoplasmic cylinder and a delay, the OM is sealed to create the newly independent cells (60, 61). If this process is error-prone, residuals from aberrantly divided cells could become incorporated into new cell ends. The second is the extrusion of blebs containing CM. By analogy with studies conducted with vancomycin-treated *E. coli* (59), we postulate that such blebs arise from naturally occurring remodeling defects in the PG, with consequent bulging of CM into the periplasmic space due to the high osmotic pressure within the cytosol. CM bulges trapped within the periplasm could be pushed backwards to a cell end, creating the vesicular (type 4) morphotype. *B. burgdorferi* provides indirect evidence for the biological origin of cell end diversity in *T. pallidum*; CET has shown that Lyme disease spirochetes also generate unusual cell end morphologies at a high frequency (66).

The ultrastructural differences between *T. denticola* and *T. pallidum* that are discernible by CET (60) are, for the most part, rather subtle. This would suggest that the disparate metabolic capabilities (27, 44, 106) of the two organisms can be accommodated with minor modifications of the basic treponemal ultrastructural scheme. The differences in tip morphologies, on the other hand, are striking even though *T. denticola*, like *T. pallidum*, attaches in vitro in a polarized manner to a variety of cell types and extracelllular matrix components (37, 38). The *T. denticola* tip consists of a simple cone ("patella-like" structure) at the terminus of the CM (60) and closely resembles that of the saprophytic *T. primitia* (80). In contrast, the simplest *T. pallidum* end (i.e., type 1) contains far more structural complexity. Of the two organisms, *T. pallidum* is by far the more invasive, both locally and systemically (56, 68, 97). One would anticipate that *T. pallidum*'s parasitic strategy would require an attachment organelle that is not only capable of binding to receptors in many different host cell types and tissues but also is part of a complex circuitry that coordinates environmental cues arising from receptor-ligand interactions with exquisite control of the motility apparatus. The structural complexity, and perhaps diversity, of the *T. pallidum* cell end is likely a major component of the enhanced virulence program with which the syphilis spirochete evolved as it and *T. denticola* diverged from their common ancestor (83).

ACKNOWLEDGMENTS

We are deeply indebted to Nyles W. Charon for sharing his wealth of knowledge about spirochete motility and ultrastructure throughout the preparation of the manuscript. We also thank Charles Wolgemuth for his many insightful comments about spirochete motility and for his assistance with the interpretation of light microscopy images of *T. pallidum*.

This work was supported by NIH grants AI-26756 (J.D.R.) and DE017106 (J.I.) and by NIH-NICRR grant P41 RR01212, which supports the Wadsworth Center's Resource for Biological Complexity as a national biotechnological resource.

REFERENCES

1. **Antal, G. M., S. A. Lukehart, and A. Z. Meheus.** 2002. The endemic treponematoses. Microbes Infect. **4:**83–94.
2. **Arnold, K., L. Bordoli, J. Kopp, and T. Schwede.** 2006. The SWISS-MODEL workspace: a web-based environment for protein structure homology modelling. Bioinformatics **22:**195–201.
3. **Barbour, A. G.** 1984. Isolation and cultivation of Lyme disease spirochetes. Yale J. Biol. Med. **57:**521–525.
4. **Beck, J. D., P. Eke, G. Heiss, P. Madianos, D. Couper, D. Lin, K. Moss, J. Elter, and S. Offenbacher.** 2005. Periodontal disease and coronary heart disease: a reappraisal of the exposure. Circulation **112:**19–24.
5. **Belisle, J. T., M. E. Brandt, J. D. Radolf, and M. V. Norgard.** 1994. Fatty acids of *Treponema pallidum* and *Borrelia burgdorferi* lipoproteins. J. Bacteriol. **176:**2151–2157.
6. **Bharti, A. R., J. E. Nally, J. N. Ricaldi, M. A. Matthias, M. M. Diaz, M. A. Lovett, P. N. Levett, R. H. Gilman, M. R. Willig, E. Gotuzzo, and J. M. Vinetz.** 2003. Leptospirosis: a zoonotic disease of global importance. Lancet Infect. Dis. **3:**757–771.
7. **Blair, D. F., D. Y. Kim, and H. C. Berg.** 1991. Mutant MotB proteins in *Escherichia coli*. J. Bacteriol. **173:**4049–4055.
8. **Blanco, D. R., K. Reimann, J. Skare, C. I. Champion, D. Foley, M. M. Exner, R. E. W. Hancock, J. N. Miller, and J. N. Lovett.** 1994. Isolation of the outer membranes from *Treponema pallidum* and *Treponema vincentii*. J. Bacteriol. **176:**6088–6099.
9. **Bourell, K. W., W. Schulz, M. V. Norgard, and J. D. Radolf.** 1994. *Treponema pallidum* rare outer membrane proteins: analysis of mobility by freeze-fracture electron microscopy. J. Bacteriol. **176:**1598–1608.
10. **Breznak, J. A.** 2006. Termite gut spirochetes, p. 421–445. *In* J. D. Radolf and S. A. Lukehart (ed.), Pathogenic *Treponema*: molecular and cellular biology. Caister Academic Press, Norwich, United Kingdom.
11. **Brinkman, M. B., M. A. McGill, J. Pettersson, A. Rogers, P. Matejkova, D. Smajs, G. M. Weinstock, S. J. Norris, and T. Palzkill.** 2008. A novel *Treponema pallidum* antigen, TP0136, is an outer membrane protein that binds human fibronectin. Infect. Immun. **76:**1848–1857.
12. **Caimano, M. J., K. W. Bourell, T. D. Bannister, D. L. Cox, and J. D. Radolf.** 1999. The *Treponema denticola* major sheath protein is predominantly periplasmic and has only limited surface exposure. Infect. Immun. **67:**4072–4083.
13. **Caimano, M. J., R. Iyer, C. H. Eggers, C. Gonzalez, E. A. Morton, M. A. Gilbert, I. Schwartz, and J. D. Radolf.** 2007. Analysis of the RpoS regulon in *Borrelia burgdorferi* in response to mammalian host signals provides insight into RpoS function during the enzootic cycle. Mol. Microbiol. **65:**1193–1217.
14. **Cameron, C. E.** 2006. The *T. pallidum* outer membrane and outer membrane proteins, p. 237–266. *In* J. D. Radolf and S. A. Lukehart (ed.), Pathogenic *Treponema*: molecular and cellular biology. Caister Academic Press, Norwich, United Kingdom.
15. **Cameron, C. E., S. A. Lukehart, C. Castro, B. Molini, C. Godornes, and W. C. Van Voorhis.** 2000. Opsonic potential, protective capacity, and sequence conservation of the *Treponema pallidum* subspecies *pallidum* Tp92. J. Infect. Dis. **181:**1401–1413.
16. **Charon, N. W., and S. F. Goldstein.** 2002. Genetics of motility and chemotaxis of a fascinating group of bacteria: the spirochetes. Annu. Rev. Genet. **36:**47–73.
17. **Charon, N. W., S. F. Goldstein, S. M. Block, K. Curci, J. D. Ruby, J. A. Kreiling, and R. J. Limberger.** 1992. Morphology and dynamics of protruding spirochete periplasmic flagella. J. Bacteriol. **174:**832–840.
18. **Charon, N. W., S. F. Goldstein, M. Marko, C. Hsieh, L. L. Gebhardt, M. A. Motaleb, C. W. Wolgemuth, R. J. Limberger, and N. Rowe.** 2009. The flat-ribbon configuration of the periplasmic flagella of *Borrelia burgdorferi* and its relationship to motility and morphology. J. Bacteriol. **191:**600–607.
19. **Charon, N. W., C. Li, and S. F. Goldstein.** 2006. The beguiling motility of the genus *Treponema*, p. 127–146. *In* J. D. Radolf and S. A. Lukehart (ed.), Pathogenic *Treponema*: molecular and cellular biology. Caister Academic Press, Norwich, United Kingdom.
20. **Christiansen, S.** 1963. Protective layer covering pathogenic treponemata. Lancet **i:**423–425.
21. **Chun, S. Y., and J. S. Parkinson.** 1988. Bacterial motility: membrane topology of the *Escherichia coli* MotB protein. Science **239:**276–278.
22. **Cox, C. D.** 1972. Shape of *Treponema pallidum*. J. Bacteriol. **109:**943–944.
23. **Cox, D. L.** 1994. Culture of *Treponema pallidum*. Methods Enzymol. **236:**390–405.
24. **Cox, D. L., D. R. Akins, K. W. Bourell, P. Lahdenne, M. V. Norgard, and J. D. Radolf.** 1996. Limited surface exposure of *Borrelia burgdorferi* outer surface lipoproteins. Proc. Natl. Acad. Sci. USA **93:**7973–7978.
25. **Cox, D. L., D. R. Akins, S. F. Porcella, M. V. Norgard, and J. D. Radolf.** 1995. *Treponema pallidum* in gel microdroplets: a novel strategy for investigation of treponemal molecular architecture. Mol. Microbiol. **15:**1151–1164.
26. **Cox, D. L., P. Chang, A. McDowall, and J. D. Radolf.** 1992. The outer membrane, not a coat of host proteins, limits the antigenicity of virulent *Treponema pallidum*. Infect. Immun. **60:**1076–1083.
27. **Cox, D. L., and J. D. Radolf.** 2006. Metabolism of the *Treponema*, p. 61–100. *In* J. D. Radolf and S. A. Lukehart (ed.), Pathogenic *Treponema*: molecular and cellular biology. Caister Academic Press, Norwich, United Kingdom.
28. **Crowther, R. A., L. A. Amos, J. T. Finch, D. J. De Rosier, and A. Klug.** 1970. Three dimensional reconstructions of spherical viruses by Fourier synthesis from electron micrographs. Nature **226:**421–425.
29. **Deka, R. K., C. A. Brautigam, X. F. Yang, J. S. Blevins, M. Machius, D. R. Tomchick, and M. V. Norgard.** 2006. The PnrA (Tp0319; TmpC) lipoprotein represents a new family of bacterial purine nucleoside receptor encoded within an ATP-binding cassette (ABC)-like operon in *Treponema pallidum*. J. Biol. Chem. **281:**8072–8081.
30. **Deka, R. K., M. S. Goldberg, K. E. Hagman, and M. V. Norgard.** 2004. The Tp38 (TpMglB-2) lipoprotein binds glucose in a manner consistent with receptor function in *Treponema pallidum*. J. Bacteriol. **186:**2303–2308.
31. **Deka, R. K., L. Neil, K. E. Hagman, M. Machius, D. R. Tomchick, C. A. Brautigam, and M. V. Norgard.** 2004. Structural evidence that the 32-kilodalton lipoprotein (Tp32) of *Treponema pallidum* is an L-methionine-binding protein. J. Biol. Chem. **279:**55644–55650.
32. **DeMot, R., and J. Vanderleyden.** 1994. The C-terminal sequence conservation between OmpA-related outer membrane proteins and MotB suggests a common function in both gram-positive and gram-negative bacteria, possibly in the interaction of these domains with peptidoglycan. Mol. Microbiol. **12:**333–334.
33. **Desrosiers, D. C., Y. C. Sun, A. A. Zaidi, C. H. Eggers, D. L. Cox, and J. D. Radolf.** 2007. The general transition metal (Tro) and Zn^{2+} (Znu) transporters in *Treponema pallidum*: analysis of metal specificities and expression profiles. Mol. Microbiol. **65:**137–152.
34. **Dewhirst, F. E., M. A. Tamer, R. E. Ericson, C. N. Lau, V. A. Levanos, S. K. Boches, J. L. Galvin, and B. J. Paster.** 2000. The diversity of periodontal spirochetes by 16S rRNA analysis. Oral Microbiol. Immunol. **15:**196–202.
35. **Dombrowski, C., W. Kan, M. A. Motaleb, N. W. Charon, R. E. Goldstein,**

and C. W. Wolgemuth. 2009. The elastic basis for the shape of *Borrelia burgdorferi*. Biophys. J. **96:**4409–4417.
36. **Dubochet, J., M. Adrian, J. J. Chang, J. C. Homo, J. Lepault, A. W. McDowall, and P. Schultz.** 1988. Cryo-electron microscopy of vitrified specimens. Q. Rev. Biophys. **21:**129–228.
37. **Ellen, R. P.** 2006. Virulence determinants of oral treponemes, p. 357–386. *In* J. D. Radolf and S. A. Lukehart (ed.), Pathogenic *Treponema*: molecular and cellular biology. Caister Academic Press, Norwich, United Kingdom.
38. **Ellen, R. P., J. R. Dawson, and P. F. Yang.** 1994. *Treponema denticola* as a model for polar adhesion and cytopathogenicity of spirochetes. Trends Microbiol. **2:**114–119.
39. **Fenno, J. C., M. Tamura, P. M. Hannam, G. W. Wong, R. A. Chan, and B. C. McBride.** 2000. Identification of a *Treponema denticola* OppA homologue that binds host proteins present in the subgingival environment. Infect. Immun. **68:**1884–1892.
40. **Fitzgerald, T. J.** 1983. Attachment of treponemes to cell surfaces, p. 195–228. *In* R. F. Schell and D. M. Musher (ed.), Pathogenesis and immunology of treponemal infection, 1st ed. Marcel Dekker, Inc., New York, NY.
41. **Fitzgerald, T. J., R. C. Johnson, J. N. Miller, and J. A. Sykes.** 1977. Characterization of the attachment of *Treponema pallidum* (Nichols strain) to cultured mammalian cells and the potential relationship of attachment to pathogenicity. Infect. Immun. **18:**467–478.
42. **Frank, J., M. Radermacher, P. Penczek, J. Zhu, Y. Li, M. Ladjadj, and A. Leith.** 1996. SPIDER and WEB: processing and visualization of images in 3D electron microscopy and related fields. J. Struct. Biol. **116:**190–199.
43. **Fraser, C. M., S. Casjens, W. M. Huang, G. G. Sutton, R. Clayton, R. Lathigra, O. White, K. A. Ketchum, R. Dodson, E. K. Hickey, M. Gwinn, B. Dougherty, J. F. Tomb, R. D. Fleischmann, D. Richardson, J. Peterson, A. R. Kerlavage, J. Quackenbush, S. Salzberg, M. Hanson, R. van Vugt, N. Palmer, M. D. Adams, J. Gocayne, J. Weidman, T. Utterback, L. Watthey, L. McDonald, P. Artiach, C. Bowman, S. Garland, C. Fujii, M. D. Cotton, K. Horst, K. Roberts, B. Hatch, H. O. Smith, and J. C. Venter.** 1997. Genomic sequence of a Lyme disease spirochaete, *Borrelia burgdorferi*. Nature **390:**580–586.
44. **Fraser, C. M., S. J. Norris, G. M. Weinstock, O. White, G. G. Sutton, R. Dodson, M. Gwinn, E. K. Hickey, R. Clayton, K. A. Ketchum, E. Sodergren, J. M. Hardham, M. P. McLeod, S. Salzberg, J. Peterson, H. Khalak, D. Richardson, J. K. Howell, M. Chidambaram, T. Utterback, L. McDonald, P. Artiach, C. Bowman, M. D. Cotton, and J. C. Venter.** 1998. Complete genome sequence of *Treponema pallidum*, the syphilis spirochete. Science **281:**375–388.
45. **Gan, L., S. Chen, and G. J. Jensen.** 2008. Molecular organization of gram-negative peptidoglycan. Proc. Natl. Acad. Sci. USA **105:**18953–18957.
46. **Gatsos, X., A. J. Perry, K. Anwari, P. Dolezal, P. P. Wolynec, V. A. Likic, A. W. Purcell, S. K. Buchanan, and T. Lithgow.** 2008. Protein secretion and outer membrane assembly in *Alphaproteobacteria*. FEMS Microbiol. Rev. **32:**995–1009.
47. **Goldstein, S. F., N. W. Charon, and J. A. Kreiling.** 1994. *Borrelia burgdorferi* swims with a planar waveform similar to that of eukaryotic flagella. Proc. Natl. Acad. Sci. USA **91:**3433–3437.
48. **Haake, D. A.** 2000. Spirochaetal lipoproteins and pathogenesis. Microbiology **146:**1491–1504.
49. **Haake, D. A., C. J. Champion, C. Martinich, E. S. Shang, D. R. Blanco, J. N. Miller, and M. A. Lovett.** 1993. Molecular cloning and sequence analysis of the gene encoding OmpL1, a transmembrane outer membrane protein of pathogenic *Leptospira* spp. J. Bacteriol. **175:**4225–4234.
50. **Haake, D. A., and J. Matsunaga.** 2002. Characterization of the leptospiral outer membrane and description of three novel leptospiral membrane proteins. Infect. Immun. **70:**4936–4945.
51. **Hardham, J. M., and L. V. Stamm.** 1994. Identification and characterization of the *Treponema pallidum tpn50* gene, an *ompA* homolog. Infect. Immun. **62:**1015–1025.
52. **Hayes, N. S., K. E. Muse, A. M. Collier, and J. B. Baseman.** 1977. Parasitism by virulent *Treponema pallidum* of host cell surfaces. Infect. Immun. **17:** 174–186.
53. **Hazlett, K. R., D. L. Cox, M. Decaffmeyer, M. P. Bennett, D. C. Desrosiers, C. J. La Vake, M. E. La Vake, K. W. Bourell, E. J. Robinson, R. Brasseur, and J. D. Radolf.** 2005. TP0453, a concealed outer membrane protein of *Treponema pallidum*, enhances membrane permeability. J. Bacteriol. **187:** 6499–6508.
54. **Hoffmann, C., A. Leis, M. Niederweis, J. M. Plitzko, and H. Engelhardt.** 2008. Disclosure of the mycobacterial outer membrane: cryo-electron tomography and vitreous sections reveal the lipid bilayer structure. Proc. Natl. Acad. Sci. USA **105:**3963–3967.
55. **Holt, S. C.** 1978. Anatomy and chemistry of spirochetes. Microbiol. Rev. **42:**114–160.
56. **Holt, S. C., and J. L. Ebersole.** 2006. The oral spirochetes: their ecology and role in the pathogenesis of periodontal disease, p. 323–356. *In* J. D. Radolf and S. A. Lukehart (ed.), Pathogenic *Treponema*: molecular and cellular biology. Caister Academic Press, Norwich, United Kingdom.
57. **Hook, E. W., III, and R. W. Peeling.** 2004. Syphilis control: a continuing challenge. N. Engl. J. Med. **351:**121–124.
58. **Hovind-Hougen, K.** 1983. Morphology, p. 3–28. *In* R. F. Schell and D. M. Musher (ed.), Pathogenesis and immunology of treponemal infection. Marcel Dekker, New York, NY.
59. **Huang, K. C., R. Mukhopadhyay, B. Wen, Z. Gitai, and N. S. Wingreen.** 2008. Cell shape and cell-wall organization in gram-negative bacteria. Proc. Natl. Acad. Sci. USA **105:**19282–19287.
60. **Izard, J., C. E. Hsieh, R. J. Limberger, C. A. Mannella, and M. Marko.** 2008. Native cellular architecture of *Treponema denticola* revealed by cryo-electron tomography. J. Struct. Biol. **163:**10–17.
61. **Izard, J., and R. J. Limberger.** 2006. Structural and genomic features of treponemal architecture, p. 39–60. *In* J. D. Radolf and S. A. Lukehart (ed.), Pathogenic *Treponema*: molecular and cellular biology. Caister Academic Press, Norwich, United Kingdom.
62. **Izard, J., W. A. Samsonoff, M. B. Kinoshita, and R. J. Limberger.** 1999. Genetic and structural analyses of cytoplasmic filaments of wild-type *Treponema phagedenis* and a flagellar filament-deficient mutant. J. Bacteriol. **181:**6739–6746.
63. **Izard, J., W. A. Samsonoff, and R. J. Limberger.** 2001. Cytoplasmic filament-deficient mutant of *Treponema denticola* has pleiotropic defects. J. Bacteriol. **183:**1078–1084.
64. **Jepsen, O. B., K. H. Hougen, and A. Birch-Andersen.** 1968. Electron microscopy of *Treponema pallidum* Nichols. Acta Pathol. Microbiol. Scand. **74:**241–258.
65. **Jones, J. D., K. W. Bourell, M. V. Norgard, and J. D. Radolf.** 1995. Membrane topology of *Borrelia burgdorferi* and *Treponema pallidum* lipoproteins. Infect. Immun. **63:**2424–2434.
66. **Kudryashev, M., M. Cyrklaff, W. Baumeister, M. M. Simon, R. Wallich, and F. Frischknecht.** 2009. Comparative cryo-electron tomography of pathogenic Lyme disease spirochetes. Mol. Microbiol. **71:**1415–1434.
67. **Kudryashev, M., M. Cyrklaff, R. Wallich, W. Baumeister, and F. Frischknecht.** 21 August 2009. Distinct in situ structures of the *Borrelia* flagellar motor. J. Struct. Biol. [Epub ahead of print.]
68. **LaFond, R. E., and S. A. Lukehart.** 2006. Biological basis for syphilis. Clin. Microbiol. Rev. **19:**29–49.
69. **LaRocca, T. J., D. J. Holthausen, C. Hsieh, C. Renken, C. A. Mannella, and J. L. Benach.** 2009. The bactericidal effect of a complement-independent antibody is osmolytic and specific to *Borrelia*. Proc. Natl. Acad. Sci. USA **106:**10752–10757.
70. **Leis, A., B. Rockel, L. Andrees, and W. Baumeister.** 2009. Visualizing cells at the nanoscale. Trends Biochem. Sci. **34:**60–70.
71. **Li, Z., and G. J. Jensen.** 2009. Electron cryotomography: a new view into microbial ultrastructure. Curr. Opin. Microbiol. **12:**333–340.
72. **Liu, J., T. Lin, D. J. Botkin, E. McCrum, H. Winkler, and S. J. Norris.** 2009. Intact flagellar motor of *Borrelia burgdorferi* revealed by cryo-electron tomography: evidence for stator ring curvature and rotor/C ring assembly flexion. J. Bacteriol. **191:**5026–5036.
73. **Lucic, V., A. Leis, and W. Baumeister.** 2008. Cryo-electron tomography of cells: connecting structure and function. Histochem. Cell Biol. **130:**185–196.
74. **Malmstrom, J., M. Beck, A. Schmidt, V. Lange, E. W. Deutsch, and R. Aebersold.** 2009. Proteome-wide cellular protein concentrations of the human pathogen *Leptospira interrogans*. Nature **460:**762–765.
75. **Matias, V. R., A. Al-Amoudi, J. Dubochet, and T. J. Beveridge.** 2003. Cryo-transmission electron microscopy of frozen-hydrated sections of *Escherichia coli* and *Pseudomonas aeruginosa*. J. Bacteriol. **185:**6112–6118.
76. **McEwen, B. F., M. Marko, C. E. Hsieh, and C. Mannella.** 2002. Use of frozen-hydrated axonemes to assess imaging parameters and resolution limits in cryoelectron tomography. J. Struct. Biol. **138:**47–57.
77. **Milne, J. L., and S. Subramaniam.** 2009. Cryo-electron tomography of bacteria: progress, challenges and future prospects. Nat. Rev. Microbiol. **7:**666–675.
78. **Mulay, V., M. J. Caimano, D. Liveris, D. C. Desrosiers, J. D. Radolf, and I. Schwartz.** 2006. *Borrelia burgdorferi* BBA74, a periplasmic protein associated with the outer membrane, lacks porin-like properties. J. Bacteriol. in press.
79. **Murphy, G. E., J. R. Leadbetter, and G. J. Jensen.** 2006. In situ structure of the complete *Treponema primitia* flagellar motor. Nature **442:**1062–1064.
80. **Murphy, G. E., E. G. Matson, J. R. Leadbetter, H. C. Berg, and G. J. Jensen.** 2008. Novel ultrastructures of *Treponema primitia* and their implications for motility. Mol. Microbiol. **67:**1184–1195.
81. **Nikaido, H.** 1996. Outer membrane, p. 29–47. *In* F. C. Neidhart, R. Curtiss III, J. Ingraham, E. Lin, K. Low, B. Magasanik, W. Reznikoff, M. Riley, M. Schaechter, and H. Umbarger (ed.), *Escherichia coli* and *Salmonella*: cellular and molecular biology, 2nd ed. American Society for Microbiology, Washington, DC.
82. **Norris, S. J., D. L. Cox, and G. M. Weinstock.** 2001. Biology of *Treponema pallidum*: correlation of functional activities with genome sequence data. J. Mol. Microbiol. Biotechnol. **3:**37–62.
83. **Norris, S. J., and G. M. Weinstock.** 2006. Comparative genomics of spirochetes, p. 19–38. *In* J. D. Radolf and S. A. Lukehart (ed.), Pathogenic *Treponema*: molecular and cellular biology. Caister Academic Press, Norwich, United Kingdom.
84. **Ovcinnikov, N. M., and V. V. Delektorskij.** 1969. Further studies of the

morphology of *Treponema pallidum* under the electron microscope. Br. J. Vener. Dis. **45:**87–116.
85. **Parsons, L. M., F. Lin, and J. Orban.** 2006. Peptidoglycan recognition by Pal, an outer membrane lipoprotein. Biochem. **45:**2122–2128.
86. **Paster, B. J., and F. E. Dewhirst.** 2006. The phylogenetic diversity of the genus *Treponema*, p. 9–18. *In* J. D. Radolf and S. A. Lukehart (ed.), Pathogenic *Treponema*: molecular and cellular biology. Caister Academic Press, Norwich, United Kingdom.
87. **Paster, B. J., F. E. Dewhirst, W. G. Weisburg, L. A. Tordoff, G. J. Fraser, R. B. Hespell, T. B. Stanton, L. Zablen, L. Mandelco, and C. R. Woese.** 1991. Phylogenetic analysis of the spirochetes. J. Bacteriol. **173:**6101–6109.
88. **Penczek, P., M. Marko, K. Buttle, and J. Frank.** 1995. Double-tilt electron tomography. Ultramicroscopy **60:**393–410.
89. **Peterson, K. M., J. B. Baseman, and J. F. Alderete.** 1983. *Treponema pallidum* receptor binding proteins interact with fibronectin. J. Exp. Med. **157:**1958–1970.
90. **Pinne, M., M. Thein, K. Denker, R. Benz, J. Coburn, and S. Bergstrom.** 2007. Elimination of channel-forming activity by insertional inactivation of the p66 gene in *Borrelia burgdorferi*. FEMS Microbiol. Lett. **266:**241–249.
91. **Radermacher, M.** 1992. Weighted back projection methods, p. 91–115. *In* J. Frank (ed.), Electron tomography. Plenum Press, New York, NY.
92. **Radermacher, M., and W. Hoppe.** 1980. Properties of 3-D reconstructions from projections from conical tilting compared to single-axis tilting. Proc. Seventh Int. Congr. Electron Microsc. **1:**132–133.
93. **Radolf, J. D.** 1995. *Treponema pallidum* and the quest for outer membrane proteins. Mol. Microbiol. **16:**1067–1073.
94. **Radolf, J. D., K. W. Bourell, D. R. Akins, J. S. Brusca, and M. V. Norgard.** 1994. Analysis of *Borrelia burgdorferi* membrane architecture by freeze-fracture electron microscopy. J. Bacteriol. **176:**21–31.
95. **Radolf, J. D., J. S. Brusca, M. E. Brandt, and M. V. Norgard.** 1992. Spirochete molecular architecture and Lyme disease pathogenesis, p. 119–134. *In* S. E. Schutzer (ed.), Lyme disease: molecular and immunologic approaches. Cold Spring Harbor Laboratory Press, New York, NY.
96. **Radolf, J. D., and D. C. Desrosiers.** 2009. *Treponema pallidum*, the stealth pathogen, changes, but how? Mol. Microbiol. **72:**1081–1086.
97. **Radolf, J. D., K. R. O. Hazlett, and S. A. Lukehart.** 2006. Pathogenesis of syphilis, p. 197–236. *In* J. D. Radolf and S. A. Lukehart (ed.), Pathogenic *Treponema*: molecular and cellular biology. Caister Academic Press, Norwich, United Kingdom.
98. **Radolf, J. D., C. Moomaw, C. A. Slaughter, and M. V. Norgard.** 1989. Penicillin-binding proteins and peptidoglycan of *Treponema pallidum* subsp. *pallidum*. Infect. Immun. **57:**1248–1254.
99. **Radolf, J. D., M. V. Norgard, and W. W. Schulz.** 1989. Outer membrane ultrastructure explains the limited antigenicity of virulent *Treponema pallidum*. Proc. Natl. Acad. Sci. USA **86:**2051–2055.
100. **Radolf, J. D., E. J. Robinson, K. W. Bourell, D. R. Akins, S. F. Porcella, L. M. Weigel, J. D. Jones, and M. V. Norgard.** 1995. Characterization of outer membranes isolated from *Treponema pallidum*, the syphilis spirochete. Infect. Immun. **63:**4244–4252.
101. **Roujeinikova, A.** 2008. Crystal structure of the cell wall anchor domain of MotB, a stator component of the bacterial flagellar motor: implications for peptidoglycan recognition. Proc. Natl. Acad. Sci. USA **105:**10348–10353.
102. **Ruby, J. D., H. Li, H. Kuramitsu, S. J. Norris, S. F. Goldstein, K. F. Buttle, and N. W. Charon.** 1997. Relationship of *Treponema denticola* periplasmic flagella to irregular cell morphology. J. Bacteriol. **179:**1628–1635.
103. **Ruiz, N., D. Kahne, and T. J. Silhavy.** 2006. Advances in understanding bacterial outer-membrane biogenesis. Nat. Rev. Microbiol. **4:**57–66.
104. **Schulze, R. J., and W. R. Zuckert.** 2006. *Borrelia burgdorferi* lipoproteins are secreted to the outer surface by default. Mol. Microbiol. **59:**1473–1484.
105. **Sequeira, P. J.** 1956. The morphology of *Treponema pallidum*. Lancet **271:**749.
106. **Seshadri, R., G. S. Myers, H. Tettelin, J. A. Eisen, J. F. Heidelberg, R. J. Dodson, T. M. Davidsen, R. T. DeBoy, D. E. Fouts, D. H. Haft, J. Selengut, Q. Ren, L. M. Brinkac, R. Madupu, J. Kolonay, S. A. Durkin, S. C. Daugherty, J. Shetty, A. Shvartsbeyn, E. Gebregeorgis, K. Geer, G. Tsegaye, J. Malek, B. Ayodeji, S. Shatsman, M. P. McLeod, D. Smajs, J. K. Howell, S. Pal, A. Amin, P. Vashisth, T. Z. McNeill, Q. Xiang, E. Sodergren, E. Baca, G. M. Weinstock, S. J. Norris, C. M. Fraser, and I. T. Paulsen.** 2004. Comparison of the genome of the oral pathogen *Treponema denticola* with other spirochete genomes. Proc. Natl. Acad. Sci. USA **101:**5646–5651.
107. **Shevchenko, D. V., D. R. Akins, E. J. Robinson, M. Li, O. V. Shevchenko, and J. D. Radolf.** 1997. Identification of homologs for thioredoxin, peptidyl prolyl *cis-trans* isomerase, and glycerophosphodiester phosphodiesterase in outer membrane fractions from *Treponema pallidum*, the syphilis spirochete. Infect. Immun. **65:**4179–4189.
108. **Skare, J. T., E. S. Shang, D. M. Foley, D. R. Blanco, C. I. Champion, T. Mirzabekov, Y. Sokolov, B. L. Kagan, J. M. Miller, and M. A. Lovett.** 1995. Virulent strain associated outer membrane proteins of *Borrelia burgdorferi*. J. Clin. Investig. **96:**2380–2392.
109. **Steere, A. C., J. Coburn, and L. Glickstein.** 2004. The emergence of Lyme disease. J. Clin. Investig. **113:**1093–1101.
110. **Steere, A. C., R. L. Grodzicki, J. E. Craft, M. Shrestha, A. N. Kornblatt, and S. E. Malawista.** 1984. Recovery of Lyme disease spirochetes from patients. Yale J. Biol. Med. **57:**557–560.
111. **Takayama, K., R. J. Rothenberg, and A. G. Barbour.** 1987. Absence of lipopolysaccharide in the Lyme disease spirochete, *Borrelia burgdorferi*. Infect. Immun. **55:**2311–2313.
112. **Thein, M., I. Bunikis, K. Denker, C. Larsson, S. Cutler, M. Drancourt, T. G. Schwan, R. Mentele, F. Lottspeich, S. Bergstrom, and R. Benz.** 2008. Oms38 is the first identified pore-forming protein in the outer membrane of relapsing fever spirochetes. J. Bacteriol. **190:**7035–7042.
113. **Thomas, D. D., J. B. Baseman, and J. F. Alderete.** 1985. Fibronectin mediates *Treponema pallidum* cytadherence through recognition of fibronectin cell-binding domain. J. Exp. Med. **161:**514–525.
114. **Thomas, D. D., M. Navab, D. A. Haake, A. M. Fogelman, J. N. Miller, and M. A. Lovett.** 1988. *Treponema pallidum* invades intercellular junctions of endothelial cell monolayers. Proc. Natl. Acad. Sci. USA **85:**3608–3612.
115. **Tilly, K., P. A. Rosa, and P. E. Stewart.** 2008. Biology of infection with *Borrelia burgdorferi*. Infect. Dis. Clin. North Am. **22:**217–234.
116. **Vollmer, W., D. Blanot, and M. A. de Pedro.** 2008. Peptidoglycan structure and architecture. FEMS Microbiol. Rev. **32:**149–167.
117. **Walker, E. M., L. A. Borenstein, D. R. Blanco, J. N. Miller, and M. A. Lovett.** 1991. Analysis of outer membrane ultrastructures of pathogenic *Treponema* and *Borrelia* species by freeze-fracture electron microscopy. J. Bacteriol. **173:**5585–5588.
118. **Walker, E. M., G. A. Zampighi, D. R. Blanco, J. N. Miller, and M. A. Lovett.** 1989. Demonstration of rare protein in the outer membrane of *Treponema pallidum* subsp. *pallidum* by freeze-fracture analysis. J. Bacteriol. **171:**5005–5011.
119. **Wang, X. G., J. M. Kidder, J. P. Scagliotti, M. S. Klempner, R. Noring, and L. T. Hu.** 2004. Analysis of differences in the functional properties of the substrate binding proteins of the *Borrelia burgdorferi* oligopeptide permease (*opp*) operon. J. Bacteriol. **186:**51–60.
120. **Wiegand, S. E., P. L. Strobel, and L. H. Glassman.** 1972. Electron microscopic anatomy of pathogenic *Treponema pallidum*. J. Investig. Dermatol. **58:**186–204.
121. **Willcox, R. R., and T. Guthe.** 1966. *Treponema pallidum*. A bibliographical review of the morphology, culture and survival of *T. pallidum* and associated organisms. Bull. W. H. O. **35:**1–169.
122. **Wolgemuth, C. W., N. W. Charon, S. F. Goldstein, and R. E. Goldstein.** 2006. The flagellar cytoskeleton of the spirochetes. J. Mol. Microbiol. Biotechnol. **11:**221–227.
123. **Wu, Y., F. L. Yeh, F. Mao, and E. R. Chapman.** 2009. Biophysical characterization of styryl dye-membrane interactions. Biophys. J. **97:**101–109.
124. **You, Y., S. Elmore, L. L. Colton, C. Mackenzie, J. K. Stoops, G. M. Weinstock, and S. J. Norris.** 1996. Characterization of the cytoplasmic filament protein gene (*cfpA*) of *Treponema pallidum* subsp. *pallidum*. J. Bacteriol. **178:**3177–3187.
125. **Zaremba, M., R. Gorska, P. Suwalski, and J. Kowalski.** 2007. Evaluation of the incidence of periodontitis-associated bacteria in the atherosclerotic plaque of coronary blood vessels. J. Periodontol. **78:**322–327.